AFCRL-69-0188

SRRC-CR-69-9

A STUDY ON SOME EQUIPMENT AND ENVIRONMENTAL PARAMETERS AFFECTING AIRBORNE REMOTE PROBING OF TEMPERATURE AND PRESSURE PROFILES

by

Wayne D. Mount, B. Richard Fow
and Charles M. Maloy

Contract No. F19628-68-C-0295
Project No. 6020
Task No. 602003
Work Unit No. 60200301

FINAL REPORT

Period Covered: 15 March 1968 – 15 November 1968

MARCH 1969

Contract Monitor: Pio J. Petrocchi
Aerospace Instrumentation Laboratory

Prepared for

AIR FORCE CAMBRIDGE RESEARCH LABORATORIES
OFFICE OF AEROSPACE RESEARCH
UNITED STATES AIR FORCE
BEDFORD, MASSACHUSETTS 01730

SPERRY RAND RESEARCH CENTER
SUDBURY, MASSACHUSETTS 01776

64

AFCRL-69-0188 SRRC-CR-69-9

A STUDY ON SOME EQUIPMENT AND ENVIRONMENTAL PARAMETERS AFFECTING AIRBORNE REMOTE PROBING OF TEMPERATURE AND PRESSURE PROFILES

by

Wayne D. Mount, B. Richard Fow
and Charles M. Maloy

Contract No. F19628-68-C-0295
Project No. 6020
Task No. 602003
Work Unit No. 60200301

FINAL REPORT

Period Covered: 15 March 1968 – 15 November 1968

MARCH 1969

Contract Monitor: Pio J. Petrocchi
Aerospace Instrumentation Laboratory

Prepared for

AIR FORCE CAMBRIDGE RESEARCH LABORATORIES
OFFICE OF AEROSPACE RESEARCH
UNITED STATES AIR FORCE
BEDFORD, MASSACHUSETTS 01730

SPERRY RAND RESEARCH CENTER
SUDBURY, MASSACHUSETTS 01776

ABSTRACT

The physical and mathematical basis for remotely probing temperature and pressure profiles from an aircraft using a microwave radiometer are presented. The results of the previous study of this problem in which its feasibility was determined are reviewed. Instrumental effects are considered and are shown to be less of a problem than was originally anticipated, with the possible exception of the problems induced by tuning uncertainties. The effect of season, latitude, and the underlying surface on the feasibility of remote probing are investigated using a simple linear inversion scheme. It is shown that seasonal and latitudinal effects do exist, but can be minimized. The effects of the underlying surface pose problems in probing below 500 mb. A technique for determining the tropopause and the temperature conditions above it are described. In general, there are no environmental or equipment considerations that adversely affect our ability to remotely measure the temperature and pressure-height profile between the 100 and 500 mb level.

TABLE OF CONTENTS

LIST OF ILLUSTRATIONS

SECTION I

INTRODUCTION

No single upper air observational system completely satisfies all requirements. Routine observations of the vertical profile of temperature, pressure height, and humidity are made at fixed locations by carrying a radiosonde package aloft with a helium-filled balloon. These direct observations are restricted in height to about 100,000 feet, are not continuous, take about 2 hours, and it is not unusual that the last observation is made more than 100 miles downwind from the first. In addition to instrumental errors, the spatial and temporal variations of these meteorological variables mean that radiosonde observations are not truly measuring the vertical profile above the observing site. Yet the radiosonde provides our basic upper air data at fixed land stations and at a few ships at sea. There are, however, large areas over the oceans and uninhabited regions of the world where no data are available. In order to maintain a global weather capability, it is necessary to close serious gaps in the observational network. Weather reconnaissance aircraft have been used successfully for this purpose; however, quantitative observations below the venicle can presently be made at only a limited number of points and with widely varying degrees of accuracy by using an expendable dropsonde. Observations at levels above the vehicles are presently non-existent, although the use of meteorological rocketsondes is being considered. The value of each weather reconnaissance flight would be increased greatly with an indirect probing system which would measure semi-continuously, passively, and without expendable packages, the vertical distribution of the meteorological variables above and/or below the aircraft.

In a previous study[1], infrared and millimeter wave techniques were explored for remotely measuring temperature and pressure height profiles. Although in principal the infrared approach can provide greater vertical resolution, the millimeter wave approach was selected for further study because of its almost comparable performance yet greater all-weather capability. These results showed, for idealized equipment and environmental parameters,

that it was feasible to obtain a remote measure of temperature and pressure height profiles.

At this early stage in the development of remote probing techniques, it is important to obtain an indication of the magnitude and relative importance of adverse equipment and environmental effects. An exhaustive study in each of the different areas would be a major analytical and experimental effort. The same would be true for evaluating the different mathematical, statistical, or empirical techniques for translating radiometric signals into meteorological data. In the hardware area, the uncertainties due to antenna beamwidth, bandwidth, integration time, and frequency instability were investigated. The interrelation between equipment noise and redundancy among observations was explored to determine the number of linearly independent observations that can be expected for given instrument errors. The effects of season, latitude, tropopause discontinuities, and underlying surface effects on the practicability of remotely probing the temperature profile were investigated. The purpose in this small, eight-month effort was to study those equipment and environmental effects which can be analytically investigated to better define the potential and unresolved problems in remote probing from an aircraft.

SECTION II

TECHNICAL BACKGROUND

This section discusses the concept of remote probing, and presents the equations necessary to simulate what an airborne radiometer would measure for any given set of atmospheric conditions.

There are two principal absorption and emission bands in the millimeter wave region due to fine structure transitions of oxygen molecules (O_2^{16}) in the atmosphere. The peak absorption of these bands is located near 60 and 120 GHz frequency and, as shown in Fig. 1, the distribution of the absorption is quite symmetrical about the peak absorption; therefore, results obtained at one absorption value are generally applicable at more than one frequency of operation. The exact value of absorption coefficient depends upon frequency, atmospheric pressure, temperature, and the concentration of oxygen molecules. A fixed pressure altitude of 100 mb has been assumed for the weather recon vehicle. From this level down to the surface the relative concentration of oxygen to the other fixed gaseous constituents of the atmosphere is invariant. Although atmospheric temperatures vary, the extreme range of variation produces less significant effects on the absorption coefficient in comparison to the frequency and pressure effects. Figure 1 shows, graphically, the effects on the oxygen absorption coefficient of the two most significant variables, i.e., frequency and atmospheric pressure, or height above sea level. Since the absorption coefficient increases with pressure, the depth from which radiation can be received at a given frequency is far less at sea level than at 100 mb, where the weather recon vehicle is assumed to be flying. This pressure effect, coupled with the gross temperature structure in the tropopause and lower stratosphere, provides a means for the operator to select layers in the atmosphere which will contribute most to the radiometric temperatures that would be measured with a downward-looking radiometer.

The molecular oxygen absorption and emission band centered at 60 GHz

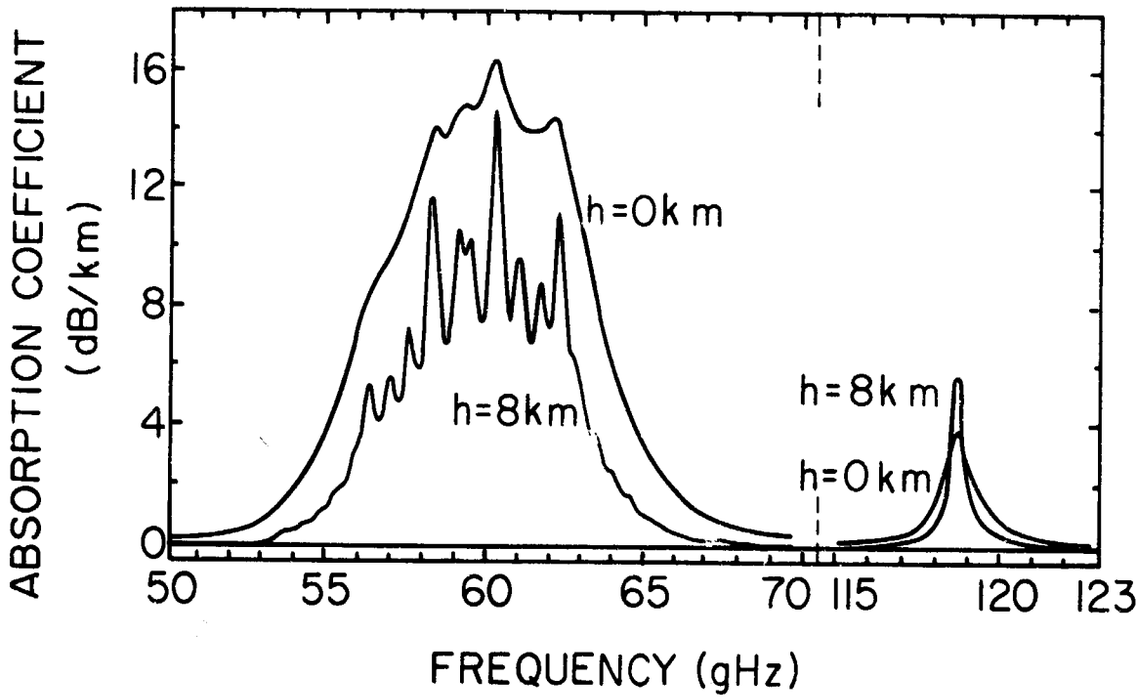

FIG. 1 Atmospheric absorption at millimeter wavelengths due to oxygen as a function of frequency and pressure altitude.

frequency, 5 mm wavelength, is due to 46 fine-structure transition lines in which the magnetic dipole moment of the molecule assumes various quantized directions with respect to its angular momentum of rotation. Since the number of lines comprising the band is rather small, an analytic expression can be used, such as Eq. (1) (after Meeks and Lilley)[2], to compute the absorption coefficient.

$$\sigma_o(\nu,P,T) = C'PT^{-3}\nu^2 \sum_N S_N \exp(-E_N/kT) \qquad (1)$$

where σ_o = absorption coefficient due to oxygen

P = atmospheric pressure

T = temperature (°K)

C' = constant (value depends upon dimensions of ν, P and desired dimensions of σ_o)

ν = frequency

S_N = pressure broadening structure factor

E_N = energy of the N^{th} rotational state

N = rotational quantum number

k = Boltzmann's constant

In addition to oxygen absorption at 60 GHz there is also absorption by the wing of the water vapor rotational transition line at 1.35 cm (ν = 22.235 GHz). However, the water vapor contribution, even down as low as 45 GHz, is rather small. The expression for the water vapor absorption coefficient suitable for use at 60 GHz was obtained from Chung[3] and is given by

$$\sigma_w = 43.2e^{-644/T} \frac{\nu^2 \rho_w}{T^{3.125}} \left(1+.011 \frac{\rho_w T}{P}\right) \left\{ \left[\frac{1}{(\nu-22.235)^2+(\Delta\nu)^2}\right] + \left[\frac{1}{(\nu+22.235)^2+(\Delta\nu)^2}\right] \right\} + 2.55 \times 10^{-3} \rho_w \nu^2 \frac{\Delta\nu}{T^{3/2}} \qquad (2)$$

where σ_w = absorption coefficient (nepers/km) due to water vapor

ρ_w = density of water vapor (g/m^3)

$\Delta\nu$ = half-width of the resonance line determined from laboratory experiments

$$= 2.61\left(1+.011\frac{\rho_w T}{P}\right)\left(\frac{P}{760}\right)\left(\frac{318}{T}\right)^{.625}$$

P = pressure (mm of Hg)

T = temperature (°K)

ν = frequency (GHz)

The transmissivity of the atmosphere is a function of the total absorption and the distance from which the energy is being received by the radiometer. The total absorption is the sum of the oxygen and water vapor contribution as given in Eq. (1) and Eq. (2). The transmissivity for a downward-looking radiometer positioned at an altitude of z_r and operating at frequency ν is given by

$$\tau_\nu = \exp\left\{-\int_{z_r}^{z} \gamma(z)\,|dz|\right\} \tag{3}$$

so that the differential transmissivity is

$$d\tau_\nu = -\gamma(z)\,\exp\left\{-\int_{z_r}^{z} \gamma(z)\,|dz|\right\}\,|dz| \tag{4}$$

It should be noted that use was made of the hydrostatic and ideal gas equation so that either height or pressure can be used as the independent variable. The solution to the radiative transfer equation can now be conveniently expressed by the following equation

$$T_{B_\nu} = \epsilon_\nu T_s \tau_{\nu_s} + r_\nu T^*_{B_\nu} \tau_{\nu_s} - \int_{P_r}^{P_0} T(P)\left\{\frac{d\tau_\nu}{d\ln P}\right\} d\ln P \tag{5}$$

where T_{B_ν} = brightness temperature or equivalent radiative temperature at frequency ν

ϵ_ν = emissivity of the underlying surface

T_s = underlying surface temperature

τ_{ν_s} = transmissivity at the underlying surface

r_ν = reflectivity of the underlying surface

$T^*_{B_\nu}$ = downward propagating radiative temperature at frequency ν

T = temperature profile expressed as a function of pressure

$\frac{d\tau_\nu}{d \ln P}$ = derivative of transmissivity at frequency ν with respect to the logarithm of pressure

The relationship between the emissivity and reflectivity is given by

$$\epsilon_\nu + r_\nu = 1 \tag{6}$$

Unfortunately, the emissive and reflective properties of various underlying surfaces have not been adequately determined for the millimeter wave region. For the initial investigation, the emissivity has been assumed to equal unity so that Eq. (5) reduces to

$$T_{B_\nu} = T_s \tau_{\nu_s} - \int_{P_r}^{P_o} T(P) \left\{ \frac{d\tau_\nu}{d\ln P} \right\} d\ln P \tag{7}$$

Further, the following relationship holds for all frequencies

$$\min[T(P)] \leq T_{B_\nu} \leq \max[T(P)] \tag{8}$$

where T is the temperature of the air or the underlying surface in the antenna beam. The equality sign holds for an isothermal profile between the radiometer and the earth's surface.

The term $\{d\tau_\nu/d\ln P\}$ in Eq. (7) is often referred to as the weighting function and expresses the relative contribution of the radiation emanating

from each layer of the atmosphere to the total amount received by the airborne radiometer. Since the weighting function depends principally on the absorption coefficient, the shape and the location of the weighting function, when plotted versus $\ln P$, are nearly independent of temperature profile. Three models of the atmosphere are presented in Fig. 2, representing cold, warm, and average temperature conditions. The weighting functions computed from these three models for four microwave frequencies are presented in Fig. 3. Figure 3 simultaneously illustrates the small temperature dependence of the weighting function and the probing of different layers in the atmosphere caused by a change in frequency. It will be shown in the next section how the weighting function concept naturally leads to a simplified scheme for the conversion of radiometric measurements to temperature profiles.

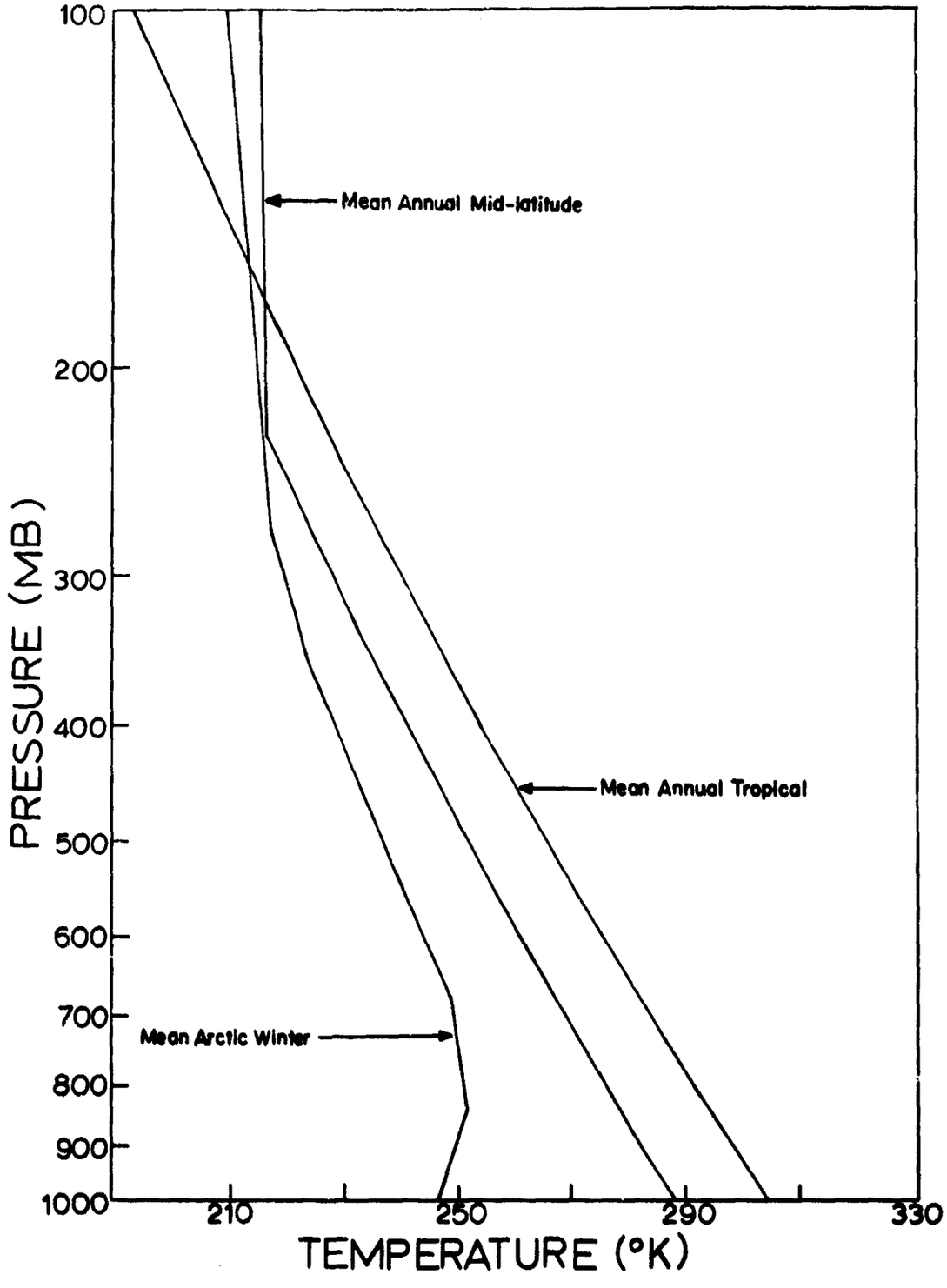

FIG. 2 Temperature-pressure profiles illustrating seasonal or annual average conditions in the tropics, mid-latitudes and arctic profiles.

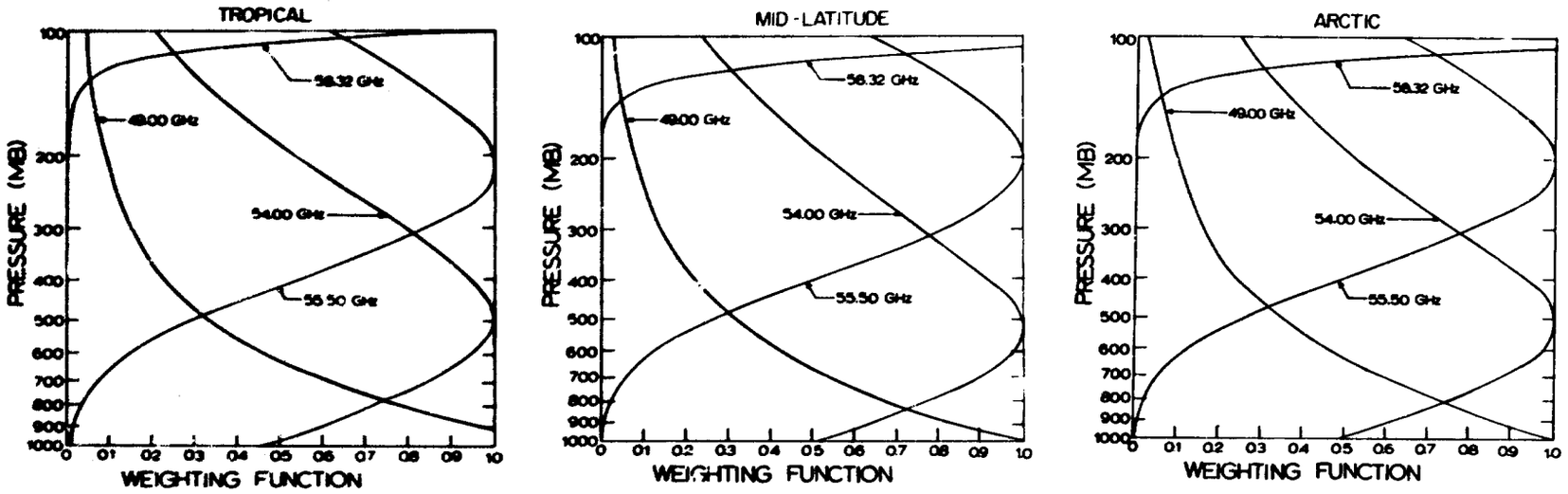

FIG. 3 Microwave weighting functions at four frequencies calculated from tropical, mid-latitude, and arctic temperature-pressure profiles.

SECTION III

DISCUSSION OF PREVIOUS RESULTS

Unique radiometric brightness temperatures can be computed from radiosonde data to simulate that which would be observed by a downward-looking radiometer operating at given frequencies. Great difficulties arise in trying to invert these brightness temperatures back to the air temperature profile from which they were computed. This problem is extremely complex, and a variety of sophisticated mathematical schemes has been proposed. Under the previous contract[4] the initial analytical feasibility of remotely probing was established using a simple empirical scheme for relating the ambient air temperature at a fixed pressure level to the brightness temperature at a given frequency.

The following three deductions can be made from the results presented in the preceeding section:

1. The brightness temperature is a weighted mean of the air temperature between the aircraft and the surface such that

$$\min[T(P)] \leq T_{B_\nu} \leq \max(T(P)]$$

2. Due to the relative temperature independence of the weighting function, the percentage contribution of the temperature profile from a given pressure layer to the total brightness temperature is nearly constant for all profiles.
3. The percentage contribution of the temperature profile from a particular pressure layer to the total brightness temperature can be varied by changing frequency.

Since the temperature profile is continuous, the first deduction implies that for all frequencies there exists a pressure level where either the ambient air or surface temperature equals the brightness temperature. The second deduction indicates that for subsequent measurements at a given frequency, the applicable pressure level (i.e., where $T(P) = T_{B_\nu}$) can be expected to be reasonably stable. The third deduction states that it is possible to select

frequencies such that radiation from different portions of the atmosphere is measured. It should, therefore, be possible to obtain a set of measurements giving some degree of vertical resolution of the temperature profile between the aircraft and the earth's surface. It should be pointed out that since the weighting function does depend to some degree upon temperature, that any fixed applicable pressure scheme will necessarily have some error. A mathematical statement of the linear scheme for translating radiometric information to air temperature data is

$$\hat{T}(P_\nu) = T_{B_\nu} + K_\nu \tag{9}$$

where $\hat{T}(P_\nu)$ = predicted ambient air temperature at the pressure level P_ν

T_{B_ν} = brightness temperature computed at frequency ν

K_ν = a constant bias associated with each frequency.

It was established that the 13 microwave frequencies have applicable pressure levels such that good vertical coverage of the temperature profile was obtained using Eq. (9). These frequencies and their corresponding applicable pressure levels and biases are presented in Table I. A statistical analysis was performed on a data sample of 20 independent temperature profiles using computed radiometric brightness temperatures for the above-mentioned 13 frequencies. The result was an average probable error of less than 1.5°C. The largest errors occurred in the lower layers of the atmosphere and in the tropopause region. These results were extremely encouraging, especially since it is not unusual for a radiosonde to have a one-degree temperature error.

A translation scheme was also developed for deriving the pressure-height profile from radiometric data. The ideal gas law in combination with the hydrostatic equation define the relationship between atmosphere pressure and geopotential height. A significant factor in the equation is the mean virtual temperature, which also contains a small contribution from the moisture in the atmosphere. The variability of water vapor, however, does not significantly affect the pressure height profiles for the 100 to 500 mb layer. This is due to the fact that in this region of the atmosphere, even

TABLE I

APPLICABLE PRESSURE LEVELS AND TEMPERATURE BIASES
FOR ALL 13 MICROWAVE FREQUENCIES

FREQUENCY (GHz)	PRESSURE (mB)	TEMP BIAS (°K)
58.3852	108	+ .1
59.9486	130	.3
57.2904	165	.6
56.0244	225	.8
55.5026	280	.2
54.9471	330	.3
54.4011	390	.1
53.8627	465	.6
53.3328	530	.6
52.8076	585	.8
51.7675	650	.8
50.2280	700	1.4
45.0	surface	1.4

under saturated conditions, the difference between the mean virtual temperature derived with and without the moisture term is only on the order of .25°C. This would amount to a maximum total error of only 12 meters in the determination of the 500 mb pressure height. Therefore, in deriving pressure-height profiles between 100 and 500 mb an accurate measure of the mean ambient dry air temperature is sufficient. It is for this reason that a method was developed for radiometrically determining the mean temperature of the 100 to 200 mb, 100 to 300 mb, and 100 to 500 mb layers. The height of the mandatory 200, 300, and 500 mb surfaces may be obtained from the thicknesses of the above layers, since it is assumed that the height of the aircraft at 100 mb is known.

As previously mentioned, the weighting function defines the relative contribution of the temperature profile from a given pressure layer to the

total brightness temperature. Further, each radiometric brightness temperature has some contribution from each of the layers of interest. It was proposed that the mean temperature of a given layer would be very nearly equal to a weighted average of the radiometric temperatures corresponding to the different frequencies where the weight would be defined from the weighting function. This method for determining the mean temperature makes use of the fact that radiometric observations are integrated quantities and not point measurements. The weight, or weighting factor, to be used for each radiometric temperature would be the area subtended by their corresponding standard atmosphere weighting functions between 100 and 200, 300, or 500 mb, depending upon which layer's mean temperature was desired. The ICAO standard atmosphere weighting functions were used for all cases because of the relative temperature independence of the weighting function. A mathematical statement of the method is

$$\bar{T}_i = \frac{\sum_{\upsilon=1}^{N} T_{B_\upsilon} \int_{100}^{P_i} \left\{ \frac{d\tau_\upsilon}{d\ln P} \right\} d\ln P}{\sum_{\upsilon=1}^{N} \int_{100}^{P_i} \left\{ \frac{d\tau_\upsilon}{d\ln P} \right\} d\ln P} + E_i \qquad (10)$$

where $\bar{T}_i$ = mean temperature of the layer 100 to P_i mb

$\{d\tau_\upsilon/d\ln P\}$ = standard atmosphere weighting function

N = number of different frequencies

P_i = 200, 300, and 500 mb for i = 1, 2, 3, respectively

E_i = residual error correction factor

The weighting factors as previously described are given by

$$WF_i(\upsilon) = \int_{100}^{P_i} \left\{ \frac{d\tau_\upsilon}{d\ln P} \right\} d\ln P \qquad (11)$$

and are listed for each frequency and pressure layer in Table II. The empirical constants E_i are given in Table III. The mean temperatures predicted by Eq. (10) were used in Eq. (12) to predict the thickness of

the layers,

$$\Delta\hat{Z}_i = \frac{R}{g}\,\bar{T}_i\,\ln\frac{P_i}{100} \qquad (12)$$

TABLE II

WEIGHTING FACTORS FOR
EACH MICROWAVE FREQUENCY

MICROWAVE FREQUENCY (GHz)	WEIGHTING FACTORS		
	100-200 (mb)	100-300 (mb)	100-500 (mb)
58.3852	1.000	1.000	1.000
59.9486	.928	.998	1.000
57.2904	.798	.974	1.000
56.0244	.700	.934	.997
55.5026	.450	.747	.956
54.9471	.295	.556	.852
54.4011	.183	.379	.685
53.8627	.112	.247	.507
53.3328	.070	.162	.360
52.8076	.047	.110	.255
51.7675	.026	.062	.149
50.2280	.015	.036	.087
45.0	.005	.012	.028

TABLE III

MICROWAVE MEAN TEMPERATURE
CORRECTION FACTORS

Region	Microwave
100-200 mb	-4.8
100-300 mb	-6.2
100-500 mb	-3.2

A statistical analysis was performed between the predicted and observed thickness of each of the 3 layers. The results are summarized in Table IV. For comparison purposes this table also contains radiosonde probable errors. The radiosonde errors increase with altitude and the reverse is true for the radiometric errors. Table IV shows that the 500, 300, and 200 mb pressure heights can be radiometrically determined with accuracies comparable to the ground-based radiosonde.

TABLE IV

COMPARISON OF HEIGHT ERRORS FROM
RADIOSONDE AND MICROWAVE RADIOMETER
FOR VARIOUS PRESSURE SURFACES

PRESSURE	RADIOMETER PROBABLE ERRORS	RADIOSONDE PROBABLE ERRORS
100	0.00 meters	45.43 meters
200	9.80	31.66
300	23.78	23.64
500	24.65	13.57

This completes the background on the schemes previously developed to translate radiometric temperatures to both temperature and pressure-height profiles. In essence, the previous results show that the temperature and pressure height profiles can be measured remotely from a weather recon vehicle. All the equations and results, however, were obtained from a limited sample of winter data only. Questions arise as to how well the results would hold for a larger independent winter data sample and to what extent seasonal, latitudinal, and equipment effects influence remote probing. These factors were explored under this contract and are presented in the next sections.

SECTION IV

INSTRUMENTAL EFFECTS

As in the case in most physical measurements, the indicated brightness temperature outputted from a radiometer is subject to errors induced by instrumental effects. Those effects which can be treated analytically are discussed, and they include the multidirectional averaging of brightness temperature due to the antenna gain pattern, frequency averaging due to the finite RF bandwidth of the radiometer, uncertainty in the frequency to which the radiometer is tuned, and the errors caused by ohmic losses in the radiometer's components. Estimates are obtained on the relative importance of these equipment effects and their implication on the ability to remotely probe temperature and pressure profiles.

Throughout this study computed brightness temperatures assume an ideal unidirectional antenna--an antenna with infinite gain in one direction and zero gain in all other directions. In reality, actual antenna gain patterns (see Fig. 4) exhibit some responsiveness in all directions around the antenna. The effect of a true gain pattern is to perform a weighted averaging of the brightness temperature from all directions, with the resultant measured quantity actually being the antenna temperature. For indirect probing to be practical, the antenna gain pattern would have to be similar to the one shown in Fig. 4, that is, the side lobes would have to be considerably less sensitive than the main lobe and the main lobe itself would have to be rather narrow. An alternate solution to this side lobe problem is to place a shroud around the antenna. The side lobes will then receive energy emanating from the shroud whose emissivity is known and whose temperature can be monitored. With this information, it is possible to account for the side lobe contribution and adjust the measured antenna temperature accordingly to obtain a more precise measure of the energy or brightness temperatures entering the main beam. It appears that existing antenna technology can satisfy the conditions necessary for remote probing. There remains the question of how much

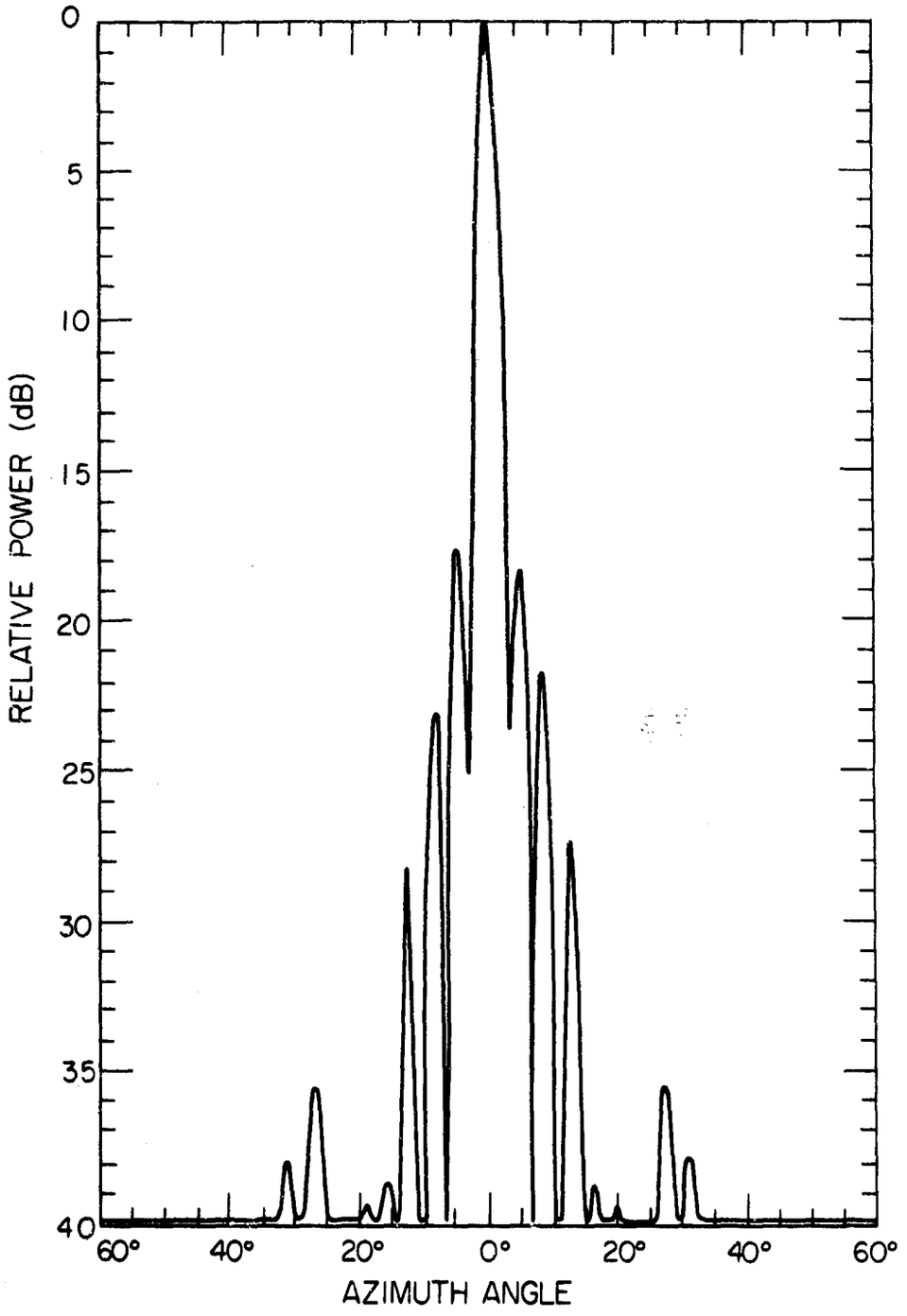

FIG. 4 A measured gain pattern for an 8" parabolic dish (Cassagrain feed) operating at 50 GHz.

different would the computed brightness temperature be if a finite antenna beamwidth were considered.

In order to investigate this question, brightness temperatures for a zero beamwidth antenna were calculated at 54.4011 GHz for several nadir angles ranging from 0° to 6°, as shown in Fig. 5. The designations (inversion and lapse) refer to the extreme types of air temperature profiles from which the brightness temperatures were calculated. The maximum range of brightness temperatures at 54.4011 GHz for the nadir angle range of 0° to 6° is less than 0.1°K. At frequencies whose absorption is stronger than that at 54.4011 GHz, even less deviation could be expected because of the corresponding decreased depth of penetration along the paths. At frequencies whose absorption is smaller than that at 54.4011 GHz, the deviation will be of the same order of magnitude if the emissivity and temperature of the underlying surface are constant. For a vehicle flying at 100 mb with a 12° beamwidth, the circular field of view on the ground surface would have a radius of about 2 km. Since the ground temperature is reasonably uniform over such a horizontal expanse, there is very little variability in brightness temperature with respect to nadir angle, and hence little deviation of brightness temperature from that measured at 0° nadir angle.

The results of the antenna gain pattern effects indicate that the uncertainties introduced by it are small in magnitude and, for our purposes at this point, the relative significance of this uncertainty will be shown to be minimal.

A more significant effect that will arise from the non-ideal nature of a real radiometer was found to be that due to the finite RF bandwidth of the radiometer and its tuning uncertainty or instability. In order to investigate these phenomena, a complete brightness temperature versus frequency spectrum was calculated using a strong lapse profile as the input temperature profile. A strong lapse case was selected, since such a temperature profile would yield a brightness temperature spectrum with very rapid changes near the transition lines, thus giving a worst possible case to consider. The resultant brightness temperature spectrum is shown in Fig. 6. Note carefully the rapid rate of change and the magnitude of the changes in brightness temperature with

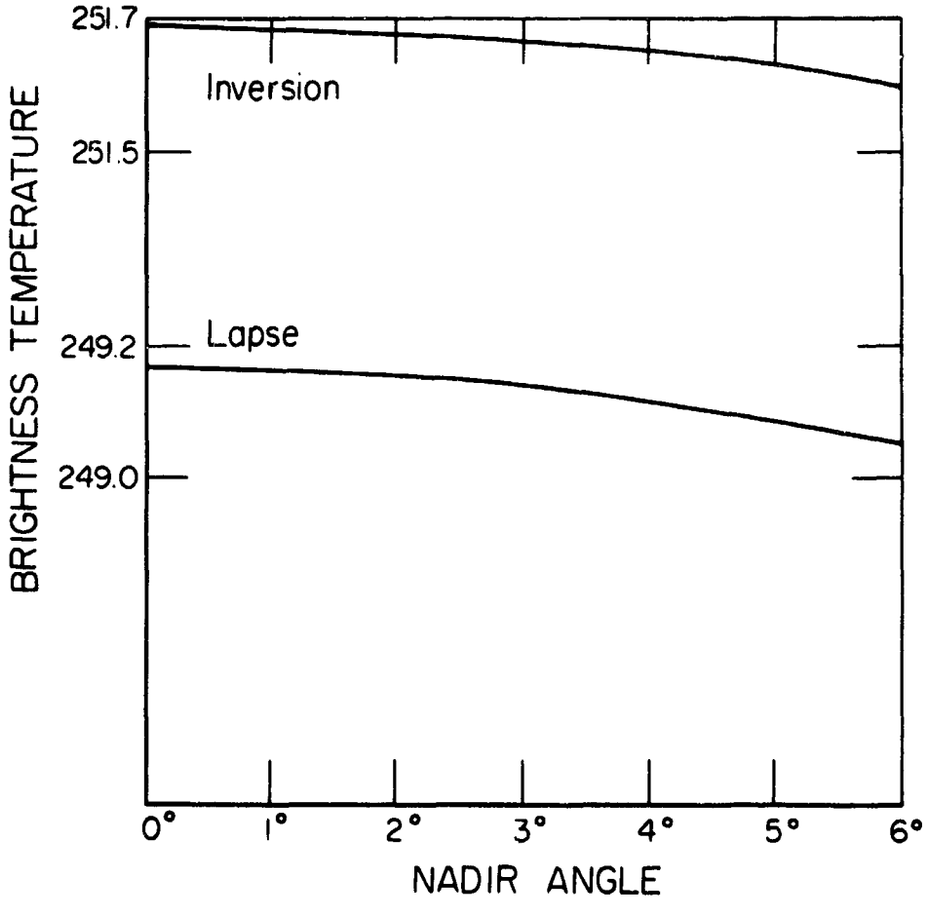

FIG. 5 Calculated brightness temperatures for lapse and inversion temperature profiles for a small range of nadir angles near 0^0 for frequency 54.4011 GHz.

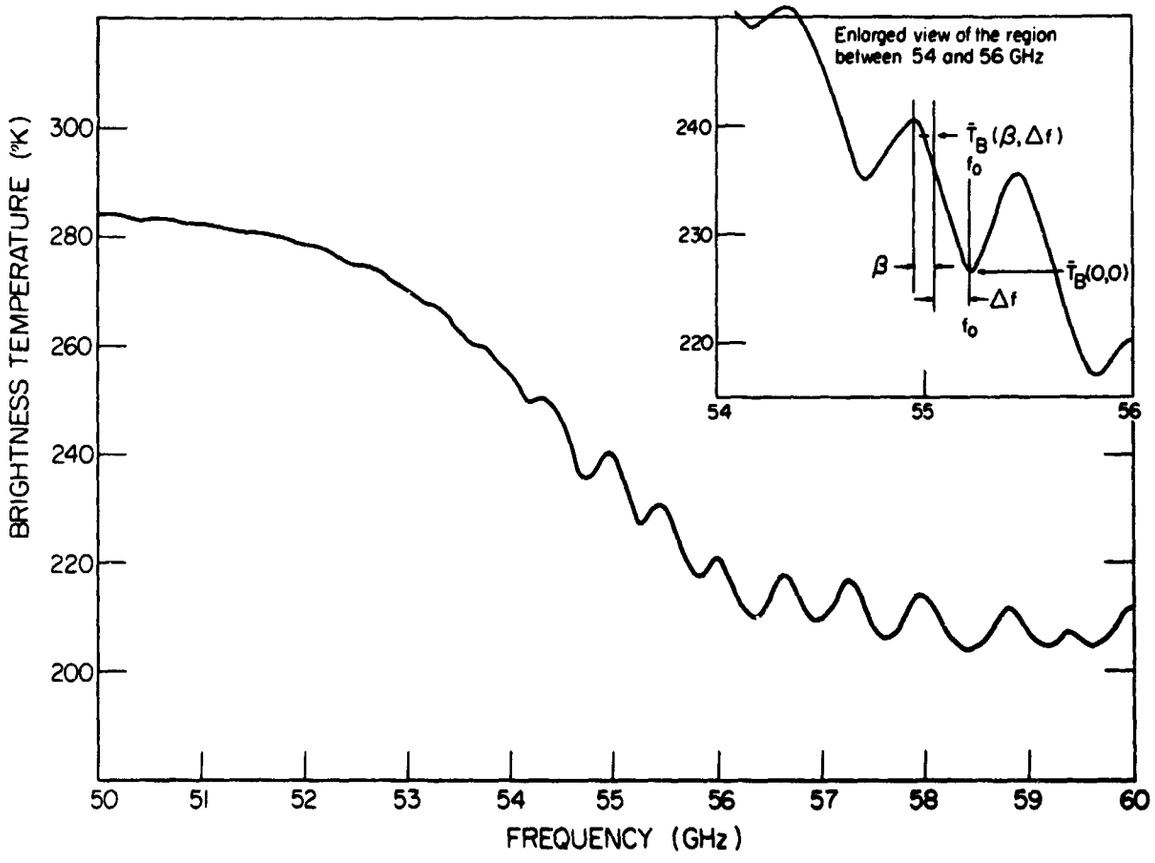

FIG. 6 Calculated brightness temperature frequency spectrum for a strong lapse temperature profile.

frequency that occur throughout the spectrum at frequencies greater than about 54 GHz. By examining the effect of bandwidth and frequency instability at the point in the spectrum where the brightness temperature changes most rapidly, an estimate of the maximum effect of these two phenomena was obtained.

A difference brightness temperature defined by Eq. (13) was calculated

$$\Delta T_B(\beta,\Delta f) = \left|\bar{T}_B(\beta,\Delta f) - \bar{T}_B(0,f_o)\right| \qquad (13)$$

$\bar{T}_B(\beta,\Delta f)$ = average brightness temperature over bandwidth β, with the bandpass offset Δf GHz from f_o

$\bar{T}_B(0,f_o)$ = brightness temperature at frequency f_o and bandwidth 0

for several bandwidths and frequency offsets from f_o = 55.221 GHz, where the most rapid change in brightness temperature with respect to frequency was noted. The frequency offsets are a means of modeling tuning uncertainty and frequency instability. The components of Eq. (13) are illustrated in Fig. 6. Note that Δf in this case is negative. The results of the calculation of $\Delta T_B(\beta,\Delta f)$ are shown in Table V. In some instances, ΔT_B was greater for positive Δf than for negative, or vise-versa. In such cases the larger of the two ΔT_B was selected and entered in the table in order to estimate the worst possible effects.

TABLE V

$\Delta T_B(\beta,\Delta f)°K$

Frequency Offset (MHz)	Bandwidth (MHz)				
	0	10	50	100	500
0	0	0	.1	.3	4.3
10	.05	0	.1	.4	4.3
20	.1	.1	.3	.6	4.2
50	1.3	1.7	1.3	1.6	4.2
100	4.1	4.5	4.1	3.8	5.3
500	11.5	11.5	11.6	12.2	13.5

The results shown in Table V indicate that frequency uncertainty, which is represented by frequency offset, is potentially a greater source of error than that due to the finite RF bandwidth of a radiometer. According to these results, an operational radiometer should probably have an RF bandwidth on the order of 50 MHz and frequency stability and tuning uncertainty of about ± 20 MHz to insure a maximum error of equal to or less than 0.3°K.

The previous discussion shows how as bandwidth increases, deviations from the desired zero bandwidth brightness temperature increase. It may be argued that this deviation is not an error and, in fact, may not be undesirable, since one could develop data analysis procedures which could interpret and make use of brightness temperatures measured with large bandwidth devices. However, the minimal effect of large bandwidth brightness temperatures is to decrease the height resolution of the derived temperature profiles and increase the possibility of redundancy in the radiometric measurements. Hence, from these considerations, narrow bandwidth measurements are most desirable; however, this particular equipment parameter lends itself to a trade-off in a total performance analysis.

Another aspect of the overall problem which places some restrictions on the lower limit of bandwidth is that relating to ΔT_{RMS}, which is the variance of the fluctuations of the indicated brightness temperature from the true brightness temperature. For a Dicke radiometer with narrow band post detection and square wave modulation operating in a null balance mode

$$\Delta T_{RMS} \approx \frac{2(T_N+T_B)}{\sqrt{Bt}} \qquad (14)$$

where T_N = radiometer system noise temperature

T_B = measured brightness temperature

B = bandwidth

t = integration time

As can be seen by inspection of Eq. (14), large bandwidths are a decided benefit, since ΔT_{RMS} varies inversely as the square root of bandwidth. Figure 7 shows a plot of ΔT_{RMS} as a function of bandwidth and integration

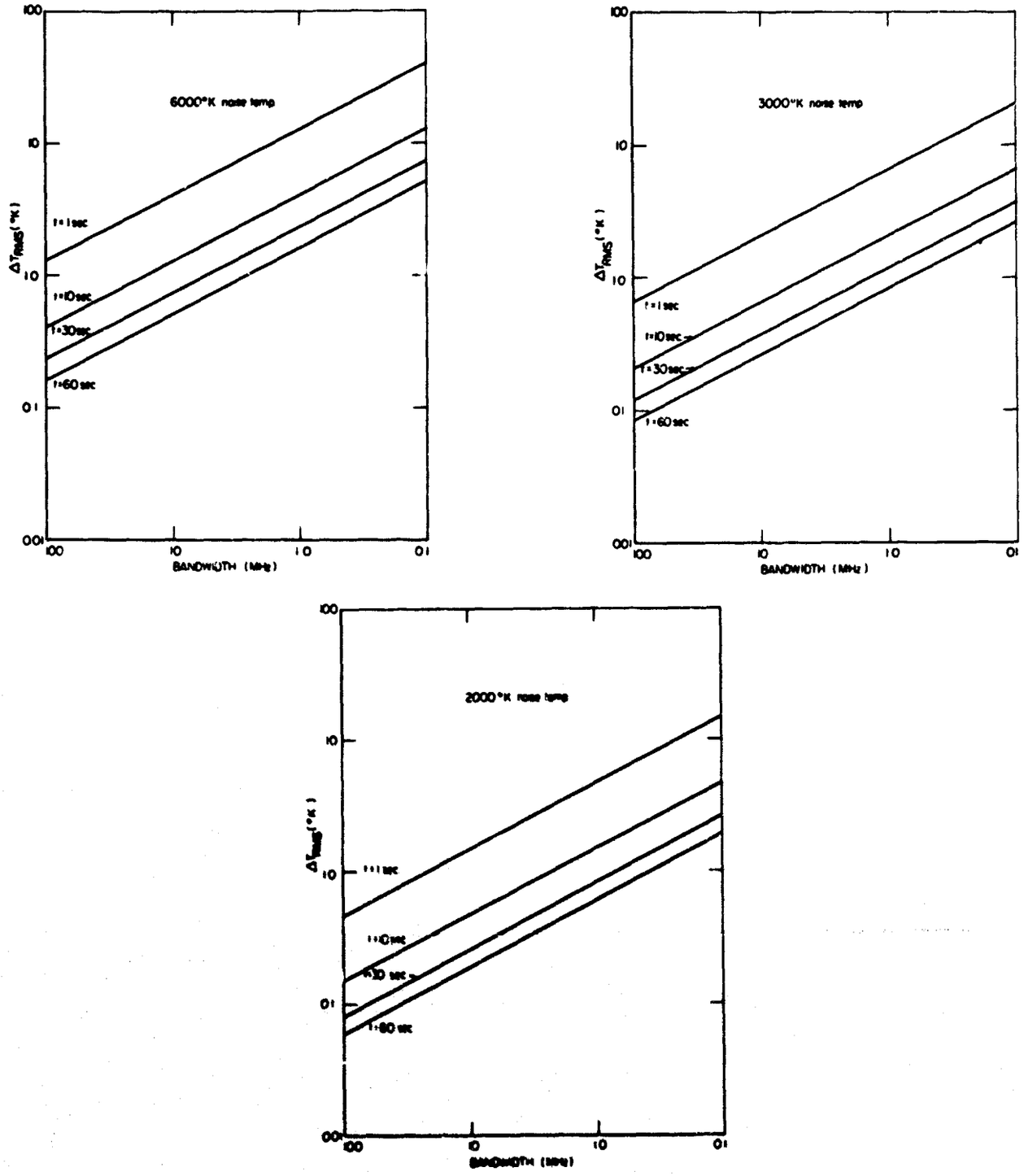

FIG. 7 Variance of brightness temperature fluctuations as a function of bandwidth and integration time for radiometers of 6000°K, 3000°K, and 2000°K system noise temperatures.

times for a 6000°K, 3000°K, and 2000°K noise temperature radiometer. These three noise temperatures represent the following levels of technological capability and relative cost in microwave radiometry.

A 6000°K noise temperature radiometer can be easily built with state of the art in radiometer technology as it exists today. A 3000°K unit represents about the upper limit of today's radiometer technology. To build such a radiometer at this time is possible but requires careful attention to details. A 2000°K radiometer represents a foreseeable level of expertise in radiometer technology within the near future.

It is evident from Fig. 7 that smaller values of ΔT_{RMS} are obtained in each of the three categories of radiometers with increasing bandwidth and/or integration time. The results of the previous considerations (summarized in Table V) indicate a 100 MHz bandwidth is the upper limit of allowable bandwidth if the errors due to bandwidth averaging and frequency uncertainty are to be kept within a selected upper limit of about 0.5°K. There are also upper limits on the allowable integration time which originate from the speed of the aircraft and its relation to the desired horizontal resolution of the sounding and the number of frequencies to be observed sequentially. If, for example, the radiometer is aboard an aircraft flying at 600 knots and ten sequential observations are required for each sounding, then to obtain a horizontal resolution of 100 miles (the order of magnitude of radiosonde resolution) a maximum possible integration time of one minute for each frequency would result. In actual practice the maximum integration time would likely be slightly less than one minute. According to the results shown in Fig. 7, integration times as small as ten seconds (when combined with bandwidths of 100 MHz) can yield ΔT_{RMS} values on the order of 0.5°K for even the 6000°K radiometer.

The trade-offs, insofar as they affect ΔT_{RMS}, between system noise temperature (which is principally cost dependent), integration time (which is determined by the mode of operation), aircraft speed and desired horizontal resolution, and bandwidth (which is in part dictated by frequency averaging errors) are thus shown in Fig. 7.

In the context of the data analysis procedure which was used in this

study (i.e., the linear translation schemes) the principal effects of errors in the radiometric data is to add to the existing uncertainty or unexplained variance. This is, however, another effect of noisy data, more subtle but perhaps more important when more sophisticated methods of data analysis are employed. The effect referred to is the interdependency or redundancy in the radiometric data which is engendered by the measurement errors. Redundancy in this case occurs when brightness temperatures at a given frequency can be calculated to an accuracy of the same order of magnitude as the measurement error from a linear combination of the other measured brightness temperatures.

This problem has been studied in detail by Twomey[5], who has developed a method for selecting from a wide choice of different measurements the maximum number of independent measurements. The criterion for the independency of the measurements is based upon the interdependency of the kernels of the associated integral equation for brightness temperature which in simplified form is

$$g(\nu) = \int_0^{z_a} \tau(z,\nu) \frac{dT(z)}{dz}\, dz \qquad (15)$$

where $g(\nu) = T_B(\nu)$ + surface contribution to the brightness temperature

$\tau(z,\nu)$ = transmission at frequency ν, from the altitude of the radiometer to altitude z

$T(z)$ = temperature profile

ν = frequency of the measurement

The transmission function $\tau(z,\nu)$ is the kernel of the integral equation. In practice, measurements are made at selected frequencies ν_i, where $i = 1,2,3,\cdots,N$. Hence the integral equation can be written as

$$g_i = \int_0^{z_a} \tau_i(z) \frac{dT(z)}{dz}\, dz \quad (i=1,2,3,\ldots,N) \qquad (16)$$

A rather complete derivation and explanation of the filtering technique used to study the redundancy and interdependency of radiometric data is given in the paper by Twomey[5]. Briefly, the method works as follows: The transmission functions $\tau_1(z), \tau_2(z), \cdots, \tau_N(z)$ provide a set of skew vectors in N dimension function-space. From these vectors an orthogonal set of function-vectors $\phi_1(z), \phi_2(z), \cdots \phi_N(z)$ and the matrix A , whose elements are given by

$$A_{ij} = \int_0^{z_a} \tau_i(z)\, \tau_j(z)\, dz \tag{17}$$

where z = altitude

z_a = altitude of radiometer

are formed. If $(U_{1j}, U_{2j}, \cdots, U_{Nj})$, $j = 1,2,\cdots,N$ are the eigenvectors of A , then the sets of functions $\vec{\tau} = (\tau_1(z), \tau_2(z), \cdots \tau_N(z))$ and $\vec{\phi}$ are related by

$$\vec{\phi} = U^{*} \vec{\tau} \tag{18}$$

$$\vec{\tau} = U \vec{\phi} \tag{19}$$

for U is an orthogonal matrix, since A is a real symmetric matrix.

It is shown by Twomey that the number of independent radiometric measurements is equal to the number of eigenvalues of A which are larger than a permissible lower bound ϵ whose value is given by

$$\epsilon = \Delta T_B / f_m \sqrt{\Delta z} \tag{20}$$

where f_m = most probable maximum value of dT/dz likely to exist in the atmosphere

Δz = height range over which $T(z)$ is being sought

ΔT_B = total uncertainty in measured brightness temperature due to all sources of random errors.

Having determined by comparing ϵ to the several eigenvalues $\lambda_1, \lambda_2, \cdots \lambda_N$ of $\|A\|$ that one or more of the radiometric observations are not independent, the problem reduces to one of finding those measurements to be eliminated which will result in the least loss of information.

The measurement to be eliminated first is the one corresponding to the $\tau_i(z)$ which is nearest to the most weakly represented base function-vector. The most weakly represented base function-vector is the particular $\phi_i(z)$ $(i=1,2,\cdots N)$ associated with the smallest eigenvalue $\lambda_i (i=1,2,\cdots,N)$. From Eq. (19) it is seen that any $\tau_i(z)$ can be resolved into a linear combination $\sum_k U_{i_k} \phi_k(z)$; the relative magnitude of the ℓ^{th} component is therefore $U_{i\ell}$. The $\tau_i(z)$ nearest to $\phi_\ell(z)$ is that for which the component, with respect to $\phi_\ell(z)$, is relatively largest. If $\phi_\ell(z)$ represents the $\phi_i(z)$ associated with the smallest eigenvalue, then the measurement to be rejected for least loss of information is, therefore, that giving rise to the largest $U_{i\ell}$. Hence the measurement selected for deletion is simply the one corresponding to the largest element of the particular eigenvector $U_{i\ell}$ associated with the smallest eigenvalue λ_ℓ.

The procedure for applying this filtering technique may be summarized as follows:

1) A complete transmission curve is computed for each frequency under consideration.
2) The matrix $\|A\| = \left\| \int_0^{z_a} \tau_i(z)\, \tau_j(t)\, dz \right\|$ is computed and the eigenvectors are found.
3) The number of eigenvalues larger than ϵ gives the number of independent pieces of information $\alpha(N)$.
4) The eigenvector corresponding to the smallest eigenvalue is then examined to find k, such that $U_{k\ell}$ is the largest of the set $\{U_{i\ell}\}$, $1=1,2,\cdots,N$.
5) The k^{th} row and column are deleted from $\|A$ to give a new A of order N-1.
6) The entire procedure is repeated for $\|A$ of order $M = N-1$, then N-2, etc. At each stage the number of independent pieces of information $\alpha(M)$ and the optimum choice of frequencies is obtained. The procedure terminates when $\alpha(M) = M$, which occurs when all of the eigenvalues are greater than ϵ.

This analysis was applied to the radiometric information calculated for the 216 RAOB data samples using a value of 10°K/km for f_m, 16 km for Δz, and .25°K for ΔT_{RMS}. The value for f_m represents our best estimate, made from an inspection of the RAOB data, for the most probable maximum vertical temperature gradient likely to be encountered. Δz is, of course, determined by the flight altitude of the aircraft, which in this case is about 16 km (100 mb level).

The results of the analysis were as follows:

(1) In all 216 cases, 6 of the 13 frequencies were found to be linearly dependent and 7 linearly independent.

(2) In over 99% of the cases, the frequencies 56.0244 and 50.2280 GHz were found to be redundant and were eliminated.

(3) In no case was 58.3852, 59.9486, 57.2904, 55.5026, or 45.000 GHz eliminated.

(4) The six frequencies most often found to be redundant (at least 38% of the cases) were 56.0244, 50.2280, 54.9471, 50.8076, 53.8627, and 51.7675 GHz.

In order to ascertain the effect of ΔT_{RMS} on the redundancy of the data, one of the cases in which the six most redundant frequencies occurred as a group was selected and rerun using a very small value of ϵ to enable us to reconstruct the maximum value of ΔT_{RMS} necessary to have caused the elimination of 1, 2, 3, ···, 12 frequencies. The results of this experiment showed that even with exceedingly small values of ΔT_{RMS} at least two frequencies would be redundant as a result of computer round-off or truncation errors. A ΔT_{RMS} on the order of .01°K was found to result in the elimination of five frequencies. One of the more surprising results of the experiment was that with ΔT_{RMS} as large as 6°K, five of the thirteen measurements would still be independent.

This work on the redundancy of data and its relationship to the random errors in the data has at least two very significant implications: (1) The minimum ΔT_{RMS} obtainable from an airborne radiometer will determine the maximum number of frequencies that a radiometer should have (unless of course deliberate redundancy is desired). In other words, there is little sense in

building a ten-frequency radiometer if as a result of the minimum RMSE of the brightness temperatures there are only seven or eight independent measurements. (2) In some data analysis schemes which may ultimately come into usage in the remote probing problem, the use of redundant data without recognizing it as such can lead to serious problems.

SECTION V

ENVIRONMENTAL EFFECTS

The potential to remotely probe the atmosphere is limited by our ability to measure precisely and to unscramble the information contained within radiometric data. Some of the important problem areas in instrumentation for remote probing have already been considered, and suitable airborne radiometric equipment appears to be within the state of the art.

Recall that a radiometric brightness temperature measurement is a weighted mean value of the air temperature throughout a layer which can be varied by varying the frequency. If each layer were not too thick and did not overlap, then it would be simple to translate brightness temperatures into air temperatures at each appropriate height and pressure level. Unfortunately, this is not the case. Thus the problem becomes one of extracting the actual temperature profile from a set of brightness temperatures which represent an overlapping set of mean temperatures. The very fact that a measure of mean temperatures is obtained means that discontinuities are smoothed. Furthermore, in the previous discussion it was shown that considerable redundancy of information exists among brightness temperature observations so that of the 13 original frequencies, only 7 were found to be linearly independent and thus capable of providing new information. The problem is further compounded in that for any given radiometric frequency, that portion of the atmosphere being interrogated varies with atmospheric density or temperature. This temperature effect is most pronounced when considering temperature profiles from different latitudes and seasons. In addition, at some frequencies the radiometric brightness temperatures contain contributions of radiation not only from oxygen molecules in the atmosphere but also from the underlying ground surface. This complicates the problem of unscrambling the brightness temperatures to obtain a remote measure of air temperature alone. The results of the influence of these environmental effects on the ability to remotely measure temperature and pressure height profiles are presented in this section.

The environmental effects will be analyzed using the simple linear schemes previously presented for translating radiometric data to obtain air temperature and pressure height profiles. Recognize that an improvement in the results presented here should be expected from application of more elegant techniques. However, development of such techniques represents a major effort. Our purpose a this time is not to develop optimum schemes for translating radiometric data, but rather to investigate what needs to be considered in developing and interpreting the results from any scheme. Therefore, the temperature errors presented should be viewed from the standpoint that better results should be attainable.

The data sample used for this analysis consisted of a total of 216 temperature, humidity, and pressure profiles occurring on 9 days between 1966 and 1968 and as observed by 24 U. S. weather stations. The weather stations were selected such that 8 stations are in each of the following three latitude bands: 25-30°N, 33-42°N, and 42-50°N latitude. The 9 days of data were selected such that there were 3 days each of winter conditions, summer conditions, and spring-fall conditions. The spring and fall seasons are considered as one seasonal grouping, since the temperature and pressure height profiles of these transitional seasons are similar. The construction of the data sample is illustrated in Table VI. The 500 mb contour maps for each day of data are presented in Fig. 8. This figure illustrates the wide variety of synoptic conditions that can exist among different seasons as well as the variety possible within a given season. The data sample is such that a statistical analysis can be performed to investigate seasonal dependence only, latitudinal dependence only, or the interaction of both season and latitude.

The linear translation scheme previously developed on winter mid-latitude data was applied to this new data sample. The probable errors in specifying the air temperature at fixed pressure levels are presented in Table VII for winter conditions in the three latitude bands. These data were obtained by computing what a radiometer would have measured at each of the 13 frequencies for each radiosonde profile, supplying the linear translation scheme to specify the air temperature at the appropriate pressure level for

TABLE VI

NUMBER OF TEMPERATURE PROFILES IN DATA SAMPLE
FROM EACH SEASON AND LATITUDE BAND FOR EACH DAY

SEASON	DATE	LATITUDE BAND			Total from Each Season
		25-33°N	33-42°N	42-50°N	
WINTER	9 January '66	8	8	8	72
	14 January '68	8	8	8	
	31 January '68	8	8	8	
SUMMER	21 July '66	8	8	8	72
	14 July '67	8	8	8	
	27 July '67	8	8	8	
SPRING-FALL	24 October '66	8	8	8	72
	1 October '67	8	8	8	
	2 April '68	8	8	8	
TOTAL FROM EACH LATITUDE BAND		72	72	72	

TABLE VII

WINTER SEASON PROBABLE TEMPERATURE ERROR (°C) FOR
EACH LATITUDE BAND USING MID-LATITUDE WINTER LINEAR TRANSLATION SCHEME

FREQUENCY (GHz)	PRESSURE (mb)	25-33°N	33-42°N	42-50°N
58.3852	108	0.31	0.45	0.30
59.9486	130	0.73	0.78	0.75
57.2904	165	1.44	1.62	1.35
56.0244	225	3.08	2.32	3.12
55.5026	280	3.86	2.09	2.41
54.9471	330	3.06	2.21	2.19
54.4011	390	1.73	1.77	2.67
53.8627	465	1.47	1.59	2.91
53.3328	530	2.22	2.18	3.19
52.8076	585	3.42	2.77	3.69
51.7675	650	7.01	3.74	4.60
50.2280	700	6.60	4.52	5.71
45.0	Surface	0.76	0.44	0.51
AVERAGE		2.75	2.04	2.57

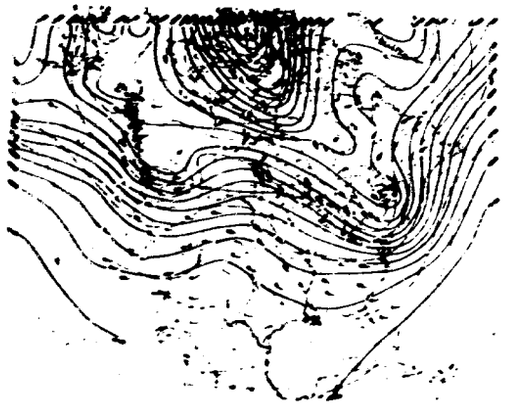

9 JANUARY 1966

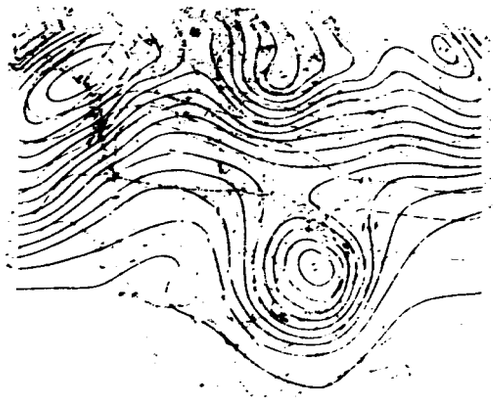

14 JANUARY 1968

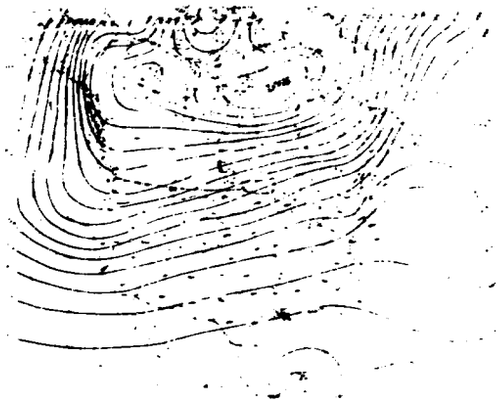

31 JANUARY 1968

21 JULY 1966

14 JULY 1967

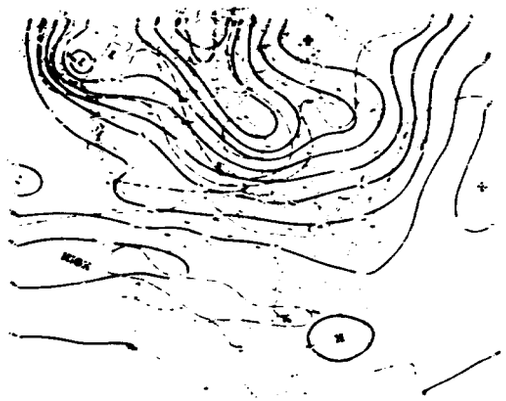

27 JULY 1967

FIG. 8 500 mb contour maps for each of the 9 days of temperature-pressure profiles comprising data sample.

each profile and deriving the statistics (probable error) applicable at each level. Notice that the scheme performs best (2.04°C error) in the mid-latitude region where it was previously developed and has the largest error (2.75°C) in the low latitude band. The vertical distribution of errors shows that the largest occur in the tropopause region (225 to 280 mb) and near the surface (below 500 mb). These are the same two problem areas previously obtained. Although the magnitude of the mid-latitude winter errors is larger than previously obtained, the vertical distribution remains the same.

To investigate what might reasonably be expected for the seasonal and latitudinal error distribution, the mid-latitude winter linear translation scheme was used as a starting point and its errors were reduced by a linear least squares refinement on the new data sample. The data sample was categorized and the least squares coefficients were developed separately for each latitude band and season. These results are presented in Table VIII where the pressure levels correspond with the same radiometric frequencies as previously presented. On the average, it can be seen that regardless of the season the linearly reduced errors increase with latitude. Also, regardless of the latitude the errors increase from summer to spring-fall, to a maximum in the winter season. The summer remote probing temperature errors are about comparable to that attainable with the radiosonde. The largest average error, winter high-latitude, is about twice that of the radiosonde; on the other hand, the largest individual value is four times larger and occurs at the first level above the surface for winter high-latitude conditions. The vertical distribution of errors is independent of latitude and season and continues to have two maxima--one associated with the temperature discontinuity in the tropopause region and another occurring between the 500 mb level and the surface. These two problem areas were investigated and are discussed in greater detail later, as will the significance of the excellent results obtained for the surface air temperature.

The data were analyzed to determine how their properties would influence most statistical schemes that might be developed to translate radiometric information into air temperature data. As background information, most of these statistical schemes operate on the principle of selecting

TABLE VIII

PROBABLE TEMPERATURE ERRORS (°C) FOR EACH SEASON AND LATITUDE BAND USING LEAST SQUARES REFINEMENT OF MID-LATITUDE WINTER LINEAR TRANSLATION SCHEME

(S = SUMMER, W = WINTER, F = SPRING-FALL)

PRESSURE (mb)	25-33°N			33-42°N			42-50°N		
	W	F	S	W	F	S	W	F	S
108	0.14	0.43	0.31	0.28	0.20	0.17	0.28	0.17	0.12
130	0.63	0.56	0.54	0.68	0.79	0.50	0.65	0.76	0.47
165	1.35	1.02	0.71	1.37	1.07	0.99	1.05	0.90	0.73
225	2.26	2.10	0.82	2.17	2.78	1.07	1.90	2.48	1.69
280	1.60	1.37	0.56	1.80	1.81	1.63	2.16	2.56	1.92
330	1.44	1.02	0.74	2.01	1.63	1.27	1.40	1.73	1.49
390	1.09	0.74	0.54	1.38	1.42	1.03	2.07	1.34	1.22
465	1.43	0.76	0.48	1.53	1.27	1.07	2.66	1.23	1.01
530	1.49	1.33	0.59	2.01	1.48	1.13	3.07	1.38	1.03
585	1.70	1.47	0.83	2.34	1.66	1.17	3.46	1.65	1.31
650	1.13	1.59	1.13	2.95	1.71	1.39	3.79	1.94	1.63
700	1.92	1.63	1.21	3.27	1.81	2.10	4.08	2.27	2.14
Surface	0.17	0.19	0.22	0.22	0.16	0.20	0.28	0.15	0.15
AVERAGE	1.26	1.09	0.67	1.70	1.37	1.06	2.07	1.43	1.15

that parameter or function which is most highly correlated or explains the greatest amount of the unexplained variance. Since the square of the correlation coefficient is a measure of the amount of variability explained, then an analysis of the correlation coefficients will apply to both of the above-listed methods for selecting optimum parameters or functions. The data sample was treated in two different ways to determine what the impact would be on the statistical properties. First, the entire data sample was used to generate the least squares refinement equations and the correlation coefficient was computed at each pressure level between the actual air tempera-

tures and those predicted by the refinement technique. Next, the data sample was categorized according to season and latitude band and the least squares refinement equations were developed for each seasonal-latitudinal category. The correlation coefficient was then computed at each pressure level for each categorized data sample between the actual air temperatures and those predicted by the refinement technique developed for that category. The correlation coefficients for all nine season-latitude categories show the same effect; therefore only those for the mid-latitude winter category, along with those obtained for the entire data sample, are presented in Table IX. Except for one level (225 mb), the correlation is higher in all cases for the translation scheme generated from the entire data sample than for that obtained from the categorized data sample. Here is an example of where the correlation coefficient is not the best criterion for choosing optimum coefficients. To apply the statistical principles discussed above for selecting parameters would result in selecting as optimum those coefficients in the equations derived from the entire data sample.

The probable temperature errors were computed on the entire data sample at each pressure level using the coefficients derived from the entire data sample. Likewise, the probable temperature errors were computed on the entire data sample at each pressure level using the appropriate coefficients that were derived from each seasonal-latitudinal categorized data sample. Table IX shows that although categorizing produces a lower correlation coefficient, total performance in producing the lowest probable error is attained with the equations derived from the categorized data samples. This shows that there is a nonlinearity involved in accounting for seasonal effects that must be considered to insure that an "optimum" statistical approach is not developed at the expense of the total available performance.

The same data sample was used to investigate the seasonal and latitudinal effects on linearly translating radiometric information to derive pressure heights. As in the previous analysis, it is assumed that the vehicle is flying at a known height at 100 mb and the radiometric observations are made at the same 13 frequencies with a zero degree nadir angle. The mid-latitude winter coefficients previously discussed for deriving the mean virtual tem-

TABLE IX

COMPARISON OF CORRELATION COEFFICIENTS AND PROBABLE TEMPERATURE ERRORS (°C) FOR ALL SEASONS, ALL LATITUDES USING LEAST SQUARES REFINEMENT WHERE THE COEFFICIENTS ARE DEVELOPED FROM ENTIRE DATA SAMPLE VS FROM SAMPLES CATEGORIZED ACCORDING TO INDIVIDUAL LATITUDE AND SEASON

PRESSURE (mb)	CORRELATION COEFFICIENTS		TEMPERATURE ERRORS WHERE LEAST SQUARES COEFFICIENTS DEVELOPED FROM	
	Entire data Sample	Winter Mid-Latitude Data Sample	Entire Data Sample	Categorized Data Sample
108	.998	.995	0.27	0.23
130	.977	.959	0.90	0.62
165	.925	.918	1.17	1.02
225	.238	.813	3.49	1.92
280	.692	.636	2.98	1.71
330	.910	.606	1.90	1.42
390	.950	.862	1.49	1.20
465	.949	.854	1.54	1.27
530	.936	.814	1.74	1.50
585	.920	.805	1.98	1.73
650	.898	.727	2.35	1.92
700	.869	.664	2.75	2.27
Surface	.9997	.9990	0.22	0.19
AVERAGE			1.75	1.31

TABLE X

WINTER SEASON PROBABLE HEIGHT ERRORS (m)
FOR EACH LATITUDE BAND USING MID LATITUDE
WINTER LINEAR TRANSLATION SCHEME

PRESSURE LEVEL	25-33°N	33-42°N	42-50°N	Radiosonde
100	0	0	0	45
200	37	25	22	32
300	29	35	32	24
500	33	27	42	14

perature between mandatory pressure levels were applied to all the winter data in this new sample. The results are presented in Table X, along with the radiosonde probable error at each pressure level. Overall, the errors are somewhat larger than previously obtained. The distribution of errors does not show any pronounced latitudinal or vertical variation. However, the mid-latitude winter coefficients do, on the average, perform slightly better in the latitude band for which they were developed. In comparison with the radiosonde errors, the 200 mb height can be specified with an accuracy slightly better than those of the radiosonde--at 300 mb they are slightly larger, and at 500 mb they are about two to three times larger than the radiosonde. Each pressure height error for each level corresponds to about 3/4°C error in radiometrically specifying the mean virtual temperature. This means that there is as large an error in specifying the mean virtual temperature from 100 to 200 mb as there is from 100 to 500 mb. A better radiometric method for specifying the temperature structure in and around the tropopause should improve the remote probing of pressure heights.

The mid-latitude winter scheme for deriving pressure heights from radiometric data was also used as a starting point and least squares refinements were again performed to investigate seasonal and latitudinal effects.

Looking first at the mid-latitude winter results in Table XI, no linear improvement was found over the independent data test presented in Table X for specifying the mid-latitude pressure height at 500 mb. This shows that no linear improvement of the previously developed scheme was possible where it was developed; however, an improvement was obtained in both the high and low latitude bands. The errors at the other levels were significantly reduced--by half at 200 mb and two-thirds at 300 mb. In general, the errors increase as the distance or difference in pressure surfaces increases. The refinement

TABLE XI

PROBABLE PRESSURE HEIGHT ERRORS (m) FOR EACH SEASON AND LATITUDE BAND USING LEAST SQUARES REFINEMENT OF MID-LATITUDE WINTER LINEAR TRANSLATION SCHEME

(S = SUMMER, W = WINTER, F = SPRING-FALL)

PRESSURE LAYER	25-33°N			33-42°N			42-50°N		
	W	F	S	W	F	S	W	F	S
100-200	11	7	5	13	12	8	13	17	7
100-300	24	17	11	12	18	14	24	19	14
100-500	24	28	20	26	36	22	32	37	17
AVERAGE	20	17	12	17	22	15	23	24	13

coefficients had a large seasonal dependency, yet the results from Table XI show that this seasonal change is reasonably accountable. In general, the 200 mb height can be specified most accurately, followed by the 300 mb height and then the 500 mb height. The results for winter and spring-fall are worse than for summer conditions and there is a slight tendency for a degradation in the high-altitude region. Overall, this least squares refinement analysis on dependent data shows the equivalent of 1/2°C error in radiometrically specifying the mean virtual temperature from 100 mb to each of the other pressure levels. These results are well within the radiosonde noise level and imply that an operational system could be developed to passively measure

the pressure height profile from 100 mb (53,000 ft.) down to the 500 mb (18,000 ft.) level.

Ground effects could adversely affect the ability to remotely probe the atmosphere. Up to now, it has been assumed that all the upwelling radiation is coming from oxygen molecules and that the emissivity of the underlying surface is unity and in thermal equilibrium with the air in contact with it. One of the most serious assumptions is that the earth is a perfect emitter, i.e., emissivity of 1.0 and reflectivity of 0.0, but the emissivity and its variability for various types of underlying surfaces has yet to be adequately measured at these frequencies. Therefore, the effects due to the maximum possible range of reflectivity values were investigated for each of the 13 frequencies used in the analysis of remote probing of temperature and pressure height profiles. The importance of knowing the surface contribution and its variability can be seen by investigating the magnitude of its effect on each frequency.

Recall that as one attempts to probe the air temperature closer and closer to the underlying surface, the magnitude of the surface contribution increases to a point where it effectively dominates the air molecule contribution. For example, at 45 GHz excellent results in specifying the surface temperatures were obtained. The effects due to the surface can be evaluated by comparing the surface transmissivity values for each frequency. As seen from Eq. (7), the surface transmissivity gives the percentage (in decimal form) of the surface temperature that is contained in the radiometric observation at any frequency. Table XII contains surface transmissivity values for each frequency as computed from 6 temperature profiles having significantly different surface pressures. The table shows that for all profiles there is a 45 to 50 per cent increase in the contribution of the surface temperature to the brightness temperature as the frequency changes from 53.3328 GHz to 50.2280 GHz. The magnitude of the surface contribution is highest at an applicable pressure of 700 mb where the brightness temperature contains between 70 and 80 per cent of the surface temperature. Thus, without an adequate measure of the surface effects, it is easy to see why it would be difficult to accurately measure remotely the 700 mb air temperature.

TABLE XII

SURFACE TRANSMISSIVITY VALUES AT EACH FREQUENCY FOR TEMPERATURE PROFILES HAVING DIFFERENT SURFACE PRESSURES (P_o)

FREQUENCY	PRESSURE	P_o = 818	P_o = 877	P_o = 925	P_o = 960	P_o = 1008	P_o = 1021
58.3852	108	.000	.000	.000	.000	.000	.000
59.9486	130	.000	.000	.000	.000	.000	.000
57.2904	165	.000	.000	.000	.000	.000	.000
56.0244	225	.000	.000	.000	.000	.000	.000
55.5026	290	.002	.001	.001	.000	.000	.000
54.9471	330	.018	.012	.008	.006	.005	.004
54.4011	390	.077	.058	.046	.039	.030	.028
53.8627	465	.195	.161	.137	.122	.102	.096
53.3328	530	.345	.302	.271	.249	.221	.210
52.8076	585	.487	.443	.410	.386	.356	.343
51.7675	650	.679	.645	.617	.594	.573	.559
50.2280	700	.809	.787	.768	.750	.740	.726
45.0	Surface	.936	.928	.921	.914	.911	.901

In addition to illustrating the rapidly changing and large surface contributions for the lower frequencies, Table XII shows that there exists significant variability in the surface contribution for different surface pressures. For a radiometric observation at frequency 53.3328 GHz, the percentage of the surface temperature contained in the observation decreases from 34.5% to 21.0% for a net decrease of 13.5% as the surface pressure increases from 818 to 1021 mb. For the other three lower frequencies, there are decreases of 14.4%, 12.0%, and 8.3% over the same surface pressure interval. Without knowledge of the surface pressure, this variability in combination with the magnitude of the surface contributions limits the temperature resolution possible in the region below 500 mb. In order to account for the variability and magnitude of the surface

contribution, it appears that a sophisticated mathematical technique will be necessary. However, it should be noted that for the usual weather reconnaissance over oceans, greater success can be expected, since the sea-level pressure variations are usually within 960 to 1025 mb, but the surface contribution in the lowest levels still predominates. This can be accounted for if the surface temperature and emissivity are known. These ground effects were evaluated by calculating the change in brightness temperature due to a change in reflectivity and emissivity from their assumed values of 0.0 and 1.0, respectively. By using Eqs. (5) and (6), the change in brightness temperature as a function of only surface reflectivity is given by

$$\Delta T_{B_\nu} = T_{B_\nu}(r_\nu) - T_{B_\nu}(r_\nu=0) = \left[\tau_{\nu_s} T_{B_\nu}^* - \tau_{\nu_s} T_s\right] r_\nu \qquad (21)$$

The above calculation was made for each of the 13 frequencies of interest using 6 different temperature-pressure profiles as model atmospheres. The results were almost identical for all profiles. Figure 9 presents a typical case of the effect of changing reflectivity on the brightness temperature that would be observed by a radiometer positioned at 100 mb.

From Fig. 9, it is immediately seen that for frequencies equal to and greater than 53.8627 GHz, the maximum possible change in brightness temperature due to reflectivity is less than 3°K. These frequencies have applicable pressures above the 500 mb level, and for reasonable values in the reflectivity variability it appears that ground effects will play a minor role in remote probing of the temperature profile between the 100 mb and 500 mb level. It is at the lower frequencies that there is a rapid increase in the reflectivity dependence of brightness temperature. These lower frequencies have applicable pressure levels below the 500 mb level, so that reflectivity may adversely affect our ability to remotely probe the temperature profile below the 500 mb level.

It is also possible that having reflectivity values greater than 0.0 may actually improve our ability to probe below the 500 mb level. From Eq. (5), it can be seen that positive values of reflectivity introduce atmospheric contributions to the brightness temperature in the form of $T_{B_\nu}^*$.

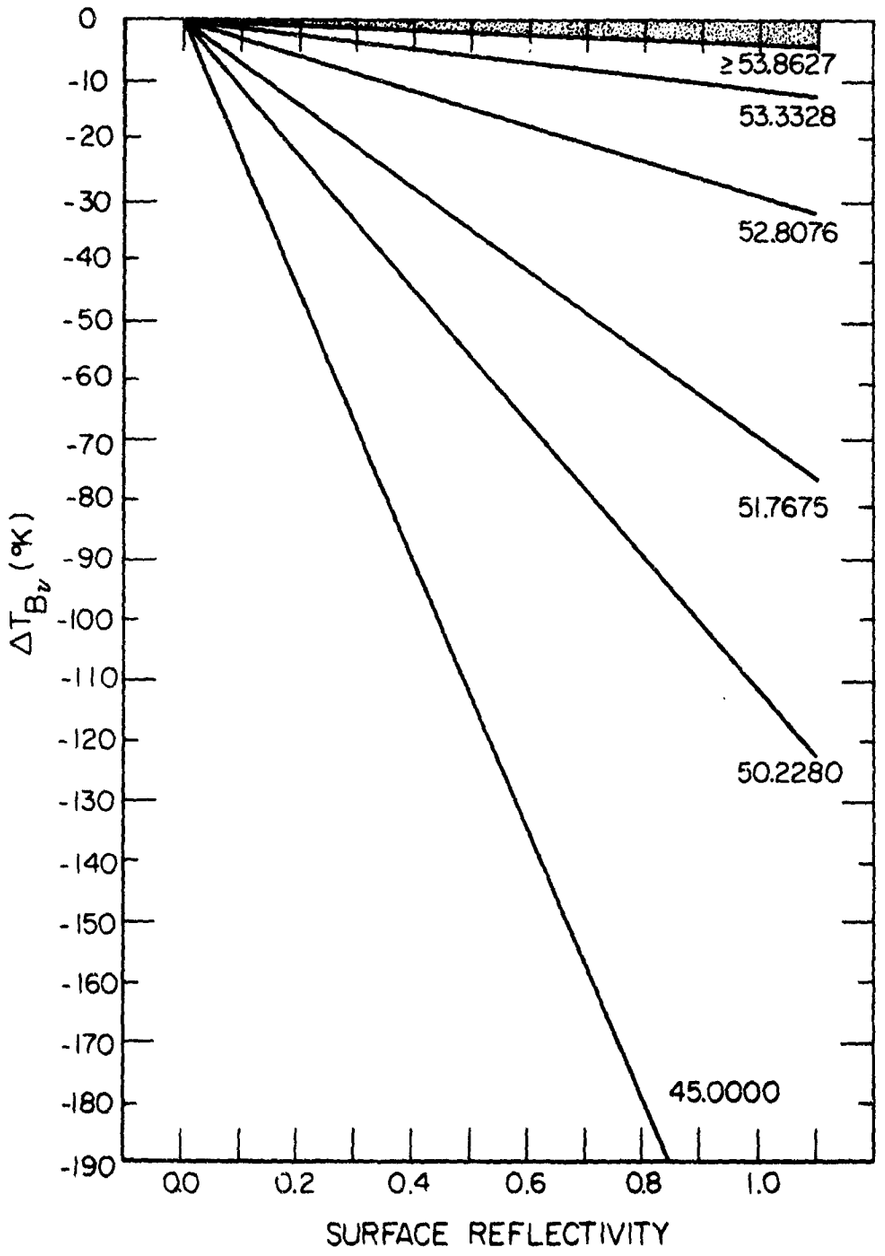

FIG. 9 Plot illustrating the change in brightness temperature due to surface reflectivity for frequencies between 45.0000 and 59.9486 GHz.

In addition, the surface contribution $\tau_{\nu_s} T_s \epsilon_\nu$ is decreased, since the emissivity decreases for increased reflectivity. In order to determine whether the ultimate effect of reflectivity would be beneficial or harmful, reflectivity values and their variability must be measured for a variety of possible underlying surfaces. The importance of the variability can be seen in Fig. 9 by the fact that a change of only 0.1 in the reflectivity causes a change of better than 22°K in the brightness temperature at 45 GHz. It can be seen that the excellent results obtained at 45 GHz for measuring the surface temperature are completely dependent upon knowing the variability of the surface reflectivity. Measurements should be made on the magnitude and variability of this parameter. Any technique for translating radiometric data can only be as good as the input data and unless effort is devoted to resolving this problem, it appears that it will not be possible to properly unscramble the radiometric signals and derive more accurate low-level temperature measurements.

Tropopause discontinuities caused significant errors in remotely probing temperature and pressure height profiles. In addition, the existence, height, and intensity of the tropopause are operationally important parameters. Different equipment modes of operation were investigated to determine the radiometric response that would be obtained for different conditions in which no tropopause exists (lapse) and in which a tropopause exists at 200 mb with isothermal and inversion profiles above it. The temperature profiles in Fig. 10 illustrate the lapse, isothermal, and inversion conditions used in this study. The two equipment modes of operation investigated were the fixed-frequency angle scanning and the fixed-angle frequency scanning. Up to now all the results presented are for the latter mode of operation. Table XIII has the brightness temperatures tabulated for the three different profiles using the fixed angle (0° nadir angle) frequency scanning mode of operation. For lapse conditions, as frequency decreases the corresponding brightness temperature increases showing that the depth of the atmosphere under interrogation is likewise increased. For isothermal and inversion conditions, the brightness temperatures likewise increase but each moves slowly as frequency decreases--indicating a change in the temperature profile. Also shown in

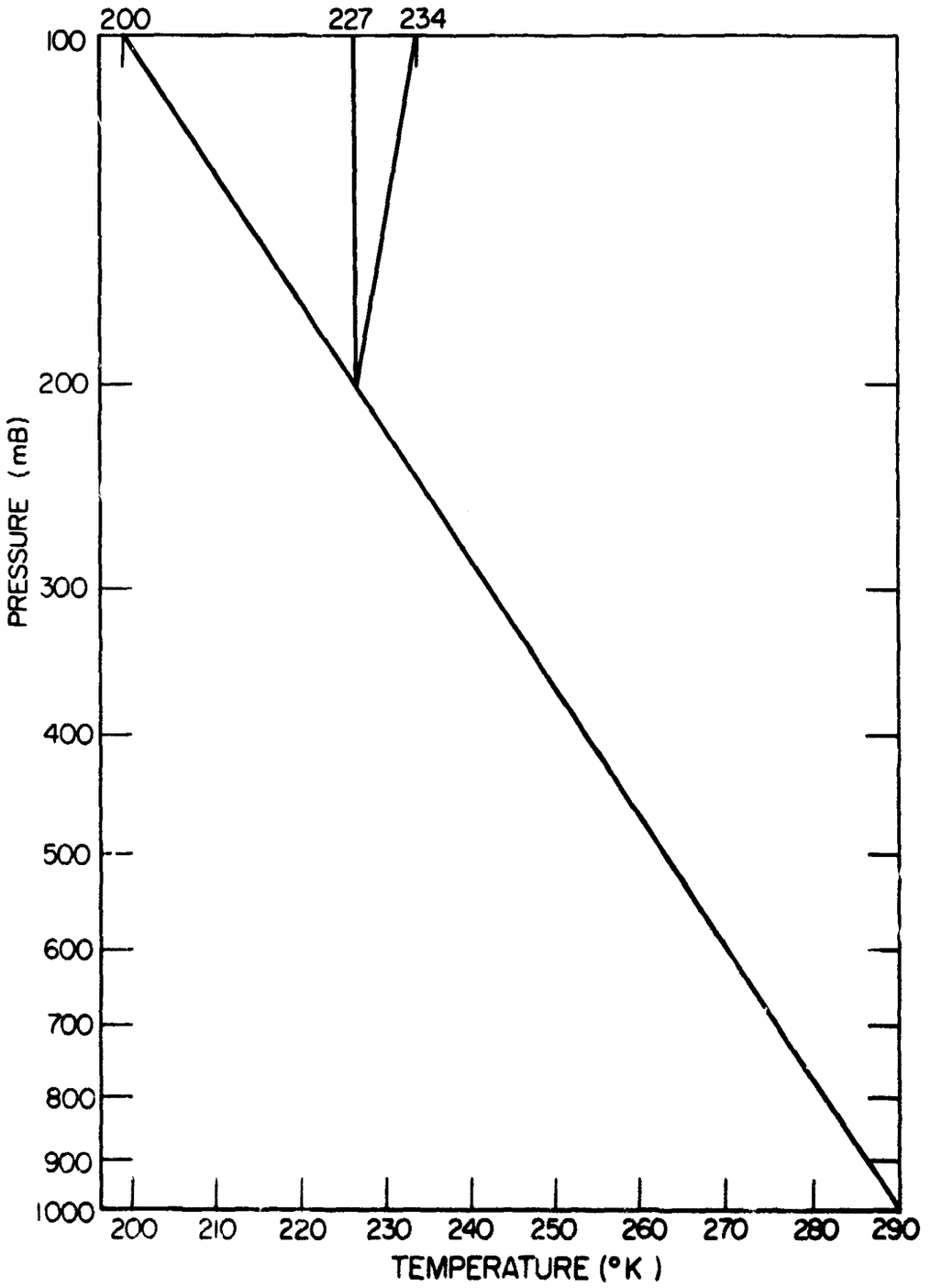

FIG. 10 Temperature profiles illustrating lapse, isothermal, and inversion conditions above the 200 mb pressure level.

TABLE XIII

RADIOMETRIC TEMPERATURES (°K) FOR A FIXED NADIR ANGLE (0°) FREQUENCY SCAN ON THREE DIFFERENT PROFILES

FREQUENCY	LAPSE	ISOTHERMAL	INVERSION	FREQUENCY REDUNDANCY
59.9455	211.0	227.3	231.1	Never
57.2904	216.2	228.7	231.6	Never
56.0244	219.6	230.1	232.7	Completely
55.5026	230.2	236.0	237.5	Never
54.9471	239.11	242.8	243.8	Partially
54.4011	249.2	252.0	251.8	Partially

Table XIII is the fact that when operating in this mode of fixed-angle frequency scanning, radiometric information at 56.0244 GHz is completely redundant and can be linearly obtained from one or more of the brightness temperatures at the other frequencies. Without the use of a technique for translating brightness temperatures to air temperatures it would be difficult to distinguish the character of the profile from this vertical sounding of radiometric temperatures.

Fixed-frequency angle scanning mode of operation was investigated as a possible means for detecting the tropopause and specifying the atmospheric conditions above and below it. For each profile, radiometric brightness temperatures were calculated at nadir angles between 75° and 0° for the same 6 frequencies. The results for the lapse, isothermal, and inversion profiles are graphically represented in Figs. 11, 12, and 13, respectively. The most striking feature is that the character of the three different profiles is immediately apparent. For the lapse profile, every frequency shows a significant and continuous brightness temperature increase from near the aircraft (75°) to vertically below (0°). For the highest frequency (59.9485) which receives radiation from air molecules closest to the antenna, a tempera-

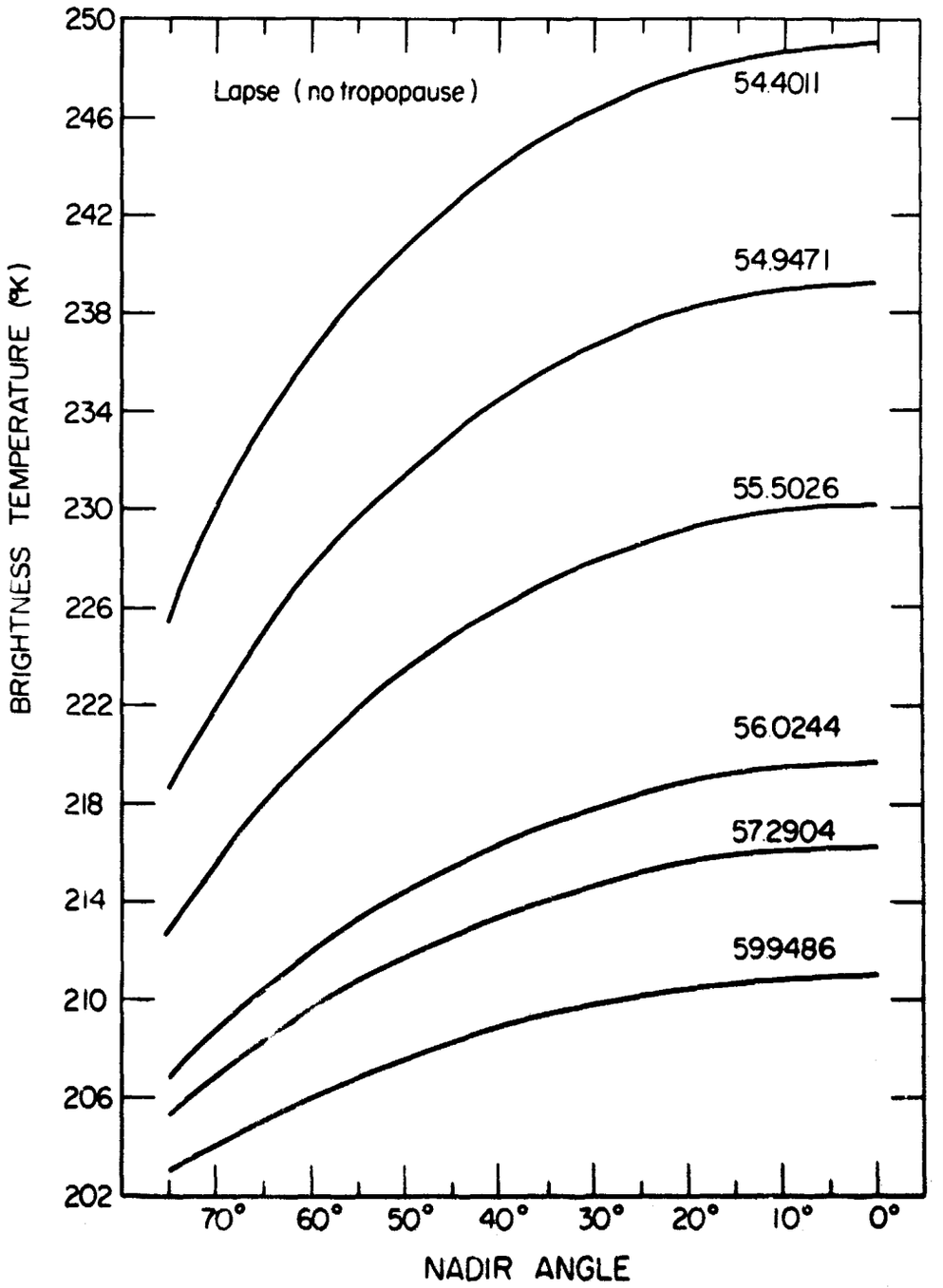

FIG. 11 Brightness temperatures at 6 frequencies vs nadir angle for completely lapse temperature profile having no tropopause below 100 mb.

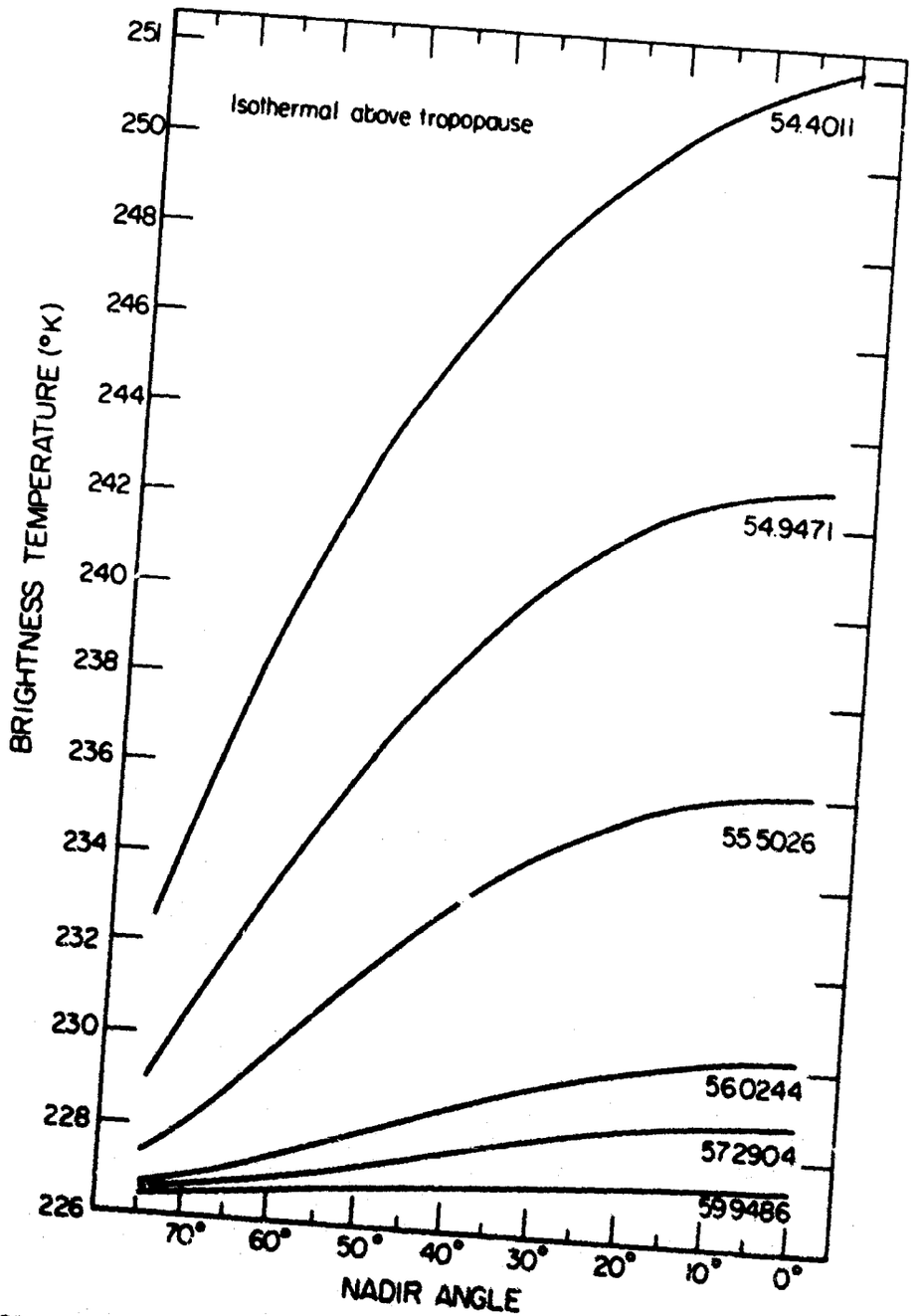

FIG. 12 Brightness temperatures at 6 frequencies vs nadir angle for lapse temperature profile having an isothermal region above the tropopause at 200 mb.

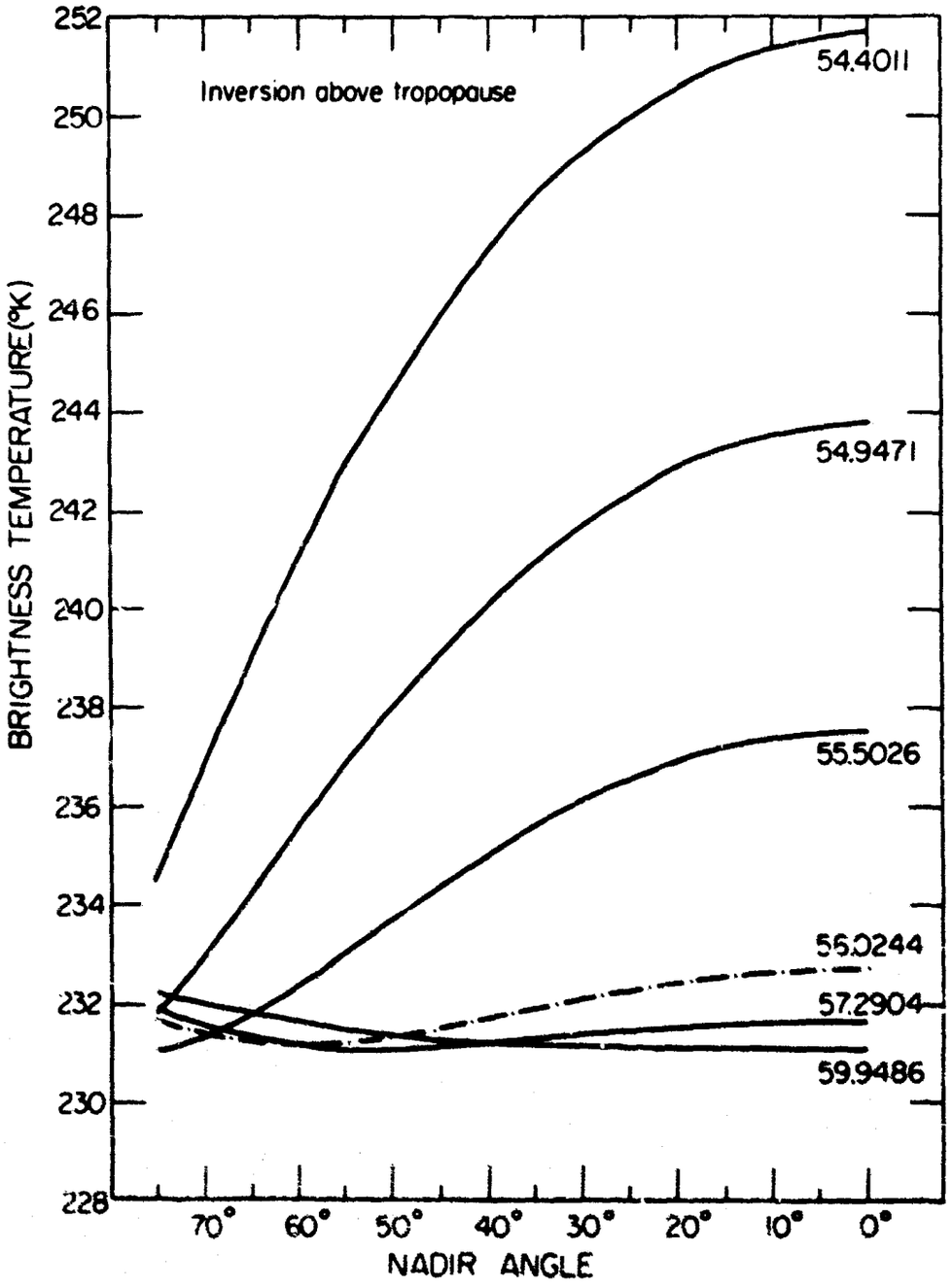

FIG. 13 Brightness temperatures at 6 frequencies vs nadir angle for lapse temperature profile having an inversion region above the tropopause at 200 mb.

ture increase of 8°K is obtained for an angle scan from 75° to 0°. For the isothermal profile, the same frequency and angle scan produced only 0.9°K temperature increase, whereas for the inversion case the same frequency angle scan gave -1.1°K temperature decrease. Thus, with the fixed-frequency angle scan mode of operation the character of the profile is immediately apparent.

In all cases, the lower frequencies are receiving information through too great a depth of the atmosphere to be responsive to the tropopause conditions. From the inversion conditions shown in Fig. 13, it can be seen that at 59.9485 GHz essentially all its information comes from levels above the tropopause. Also, it can be seen that the brightness temperatures at 56.0244 and 57.2904 GHz as a function of nadir angle are responsive to information from both above and below the tropopause, with the largest radiometric response found at 56.0244. Note that the inflection point of these curves shifts to larger nadir angles as frequency decreases. This should be expected, since each lower frequency is probing a greater depth of the atmosphere and the tropopause is therefore detected at a higher nadir angle. These results show that the existence of a tropopause, as well as the character of the temperature profile above and below the tropopause, can be obtained by use of a fixed-frequency angle scan mode of operation. This indicates that considerable reduction in the temperature and pressure height error should be possible by a better accounting of the conditions in the tropopause region and that the height and intensity of the tropopause should be measurable remotely.

In principle, fixed-angle frequency scanning should be able to provide a sequence of brightness temperatures that would depict the tropopause conditions in a manner somewhat similar to that presented for the fixed-frequency angle scan mode of operation. As discussed in the section on instrumental effects, small uncertainties in frequency tuning and absolute temperature calibration from one frequency to another will increase the number of frequencies having redundant information and thus reduce the vertical resolution. One advantage of the fixed-frequency angle scan mode is that for the same frequency offset, the relative temperature change as angle is scanned would still depict the character of the profile, though for a slightly different depth of the atmosphere; a disadvantage is that this mode requires a scanning

antenna. The operational performance of an airborne radiometer will dictate which of these modes will provide the best information on the vertical structure of the atmosphere. This is an area which should be considered in a trade-off between equipment sophistication and different modes of operation.

Recall from the instrumental effects section that the information contained within brightness temperatures measured at 56.0244 was found to be completely redundant. Thus for a frequency scan downward pointing radiometric mode of operation, this frequency would not be used to make observations, yet as previously seen in Fig. 12, the brightness temperatures at this frequency responded greatest to the atmospheric conditions above and below the tropopause--the very region in which an improvement was needed. Again, it can be seen that care must be exercised in applying the various completely statistical methods to insure that the results are interpreted properly and that the best performance is achieved.

SECTION VI

CONCLUSIONS

1. It appears that state-of-the-art technology allows for the construction of a radiometer having the necessary bandwidth, antenna gain pattern, and frequency stability to obtain sufficient accuracy in the measured radiometric brightness temperature.
2. Seasonal and latitudinal effects can be minimized by categorizing the empirical constants used in the scheme to translate radiometric information to obtain temperature nd pressure profiles.
3. Temperature profiles can be most accurately measured in the 100-500 mb region. Greater accuracy should be possible in the tropopause region by using a fixed-frequency angle scan mode of operation. Indications are that this mode of operation will show not only the existence of the tropopause but also the temperature conditions above and below it.
4. The magnitude and variability of the surface contribution to the brightness temperature make it difficult to obtain resolution below the 500 mb level. A more sophisticated scheme for translating radiometric data may be necessary to improve resolution in this region.
5. The pressure-height of the mandatory pressure levels can be successfully measured down to the 500 mb pressure level. Simple linear corrections are able to account for seasonal and latitudinal effects.
6. Ground effects present no serious problem for remotely measuring the temperature profile from the 100 to 500 mb pressure level. It will be necessary to elevate reflectivity for various underlying surfaces to determine the ground effect on remote probing below the 500 mb level.
7. In general, this study shows from an equipment and data processing point of view that it appears within the state of the art to remotely measure temperature and pressure height profiles down to 500 mb with an airborne radiometric system. An inflight experimental and data gathering program is now warranted.
8. Work on the capabilities of remotely probing temperature and pressure height profiles above a weather reconnaissance vehicle should be investigated to determine its full potential for operational utilization.

REFERENCES

1. Mount, W. D. and B. R. Fow, Results Applicable to Clear Air Turbulence Detection Using Millimeter Wave Radiometer Probe, ION-SAE Conference Proceedings, Washington, D. C., Feb. 23-24, 1966 (published by Society of Automotive Engineers, Inc., 485 Lexington Ave., New York, New York 10017).

2. Meeks, M. L. and A. E. Lilley, The Microwave Spectrum Oxygen in the Earth's Atmosphere, J. of Geophysics Res. 68(6), 1683-1703 (1963).

3. Chung, V. K., Microwave Spectrum of the Planet Venus, MS Thesis, Mass. Inst. of Tech., Dept. of Elec. Engr. (1962).

4. AFCRL Contract No. AF19(628)-6133.

5. Twomey, S., Indirect Measurement of Atmospheric Temperature Profiles from Satellites: Part II, Mathematical Aspects of the Inversion Problem, Monthly Weather Review, Vol. 94, No. 6, pp. 363-366 (1966).

UNCLASSIFIED

Security Classification

DOCUMENT CONTROL DATA - R&D

(Security classification of title, body of abstract and indexing annotation must be entered when the overall report is classified)

1 ORIGINATING ACTIVITY (Corporate author)

Sperry Rand Research Center
100 North Road
Sudbury, Massachusetts 01776

2a REPORT SECURITY CLASSIFICATION: unclassified

2b GROUP: ------

3 REPORT TITLE

A STUDY ON SOME EQUIPMENT AND ENVIRONMENTAL PARAMETERS AFFECTING AIRBORNE REMOTE PROBING OF TEMPERATURE AND PRESSURE PROFILES

4 DESCRIPTIVE NOTES (Type of report and inclusive dates)

Scientific. Final. 15 March 1968 - 15 November 1968 approved-23 May 1969.

5 AUTHOR(S) (Last name, first name, initial)

Wayne D. Mount; B. Richard Fow; Charles M. Maloy

6 REPORT DATE	7a TOTAL NO. OF PAGES	7b NO OF REFS
March 1969	63	5

8a CONTRACT OR GRANT NO. F19628-68-C-0295

b PROJECT NO Task, Work Unit Nos. 6020-03-01

c DoD Element 62101F

d DoD Subelement 681000

9a ORIGINATOR'S REPORT NUMBER(S): SRRC-CR-69-9

9b OTHER REPORT NO(S) (Any other numbers that may be assigned this report): AFCRL-69-0188

10 AVAILABILITY LIMITATION NOTICES

1 - Distribution of this document is unlimited. It may be released to the Clearinghouse, Department of Commerce, for sale to the general public.

11 SUPPLEMENTARY NOTES: TECH, OTHER

12 SPONSORING MILITARY ACTIVITY: Air Force Cambridge Research Laboratories (CRE), L. G. Hanscom Field, Bedford, Massachusetts 01730

13 ABSTRACT

The physical and mathematical basis of remotely probing temperature and pressure profiles from an aircraft using a microwave radiometer are presented. The results of the previous study of this problem in which its feasibility was determined are reviewed. Instrumental effects are considered and are shown to be less of a problem then was originally anticipated, with the possible exception of the problems induced by tuning uncertainties. The effect of season, latitude, and the underlying surface on the feasibility of remote probing are investigated using a simple linear inversion scheme. It is shown that seasonal and latitudinal effects do exist, but can be minimized. The effects of the underlying surface pose problems in probing below 500 mb. A technique for determining the tropopause and the temperature conditions above it are described. In general, there are no environmental or equipment considerations that adversely affect our ability to remotely measure the temperature and pressure-height profile between the 100 and 500 mb level.

DD FORM 1 JAN 64 1473

UNCLASSIFIED

Security Classification

14 KEY WORDS	LINK A		LINK B		LINK C	
	ROLE	WT	ROLE	WT	ROLE	WT
Remote probing						
Temperature profiles						
Pressure profiles						
Microwave						
Radiometer						
Seasonal effects						
Latitudinal effects						
Tropopause						

INSTRUCTIONS

1. ORIGINATING ACTIVITY: Enter the name and address of the contractor, subcontractor, grantee, Department of Defense activity or other organization *(corporate author)* issuing the report.

2a. REPORT SECURITY CLASSIFICATION: Enter the overall security classification of the report. Indicate whether "Restricted Data" is included. Marking is to be in accordance with appropriate security regulations.

2b. GROUP: Automatic downgrading is specified in DoD Directive 5200.10 and Armed Forces Industrial Manual. Enter the group number. Also, when applicable, show that optional markings have been used for Group 3 and Group 4 as authorized.

3. REPORT TITLE: Enter the complete report title in all capital letters. Titles in all cases should be unclassified. If a meaningful title cannot be selected without classification, show title classification in all capitals in parenthesis immediately following the title.

4. DESCRIPTIVE NOTES: If appropriate, enter the type of report, e.g., interim, progress, summary, annual, or final. Give the inclusive dates when a specific reporting period is covered.

5. AUTHOR(S): Enter the name(s) of author(s) as shown on or in the report. Enter last name, first name, middle initial. If military, show rank and branch of service. The name of the principal author is an absolute minimum requirement.

6. REPORT DATE: Enter the date of the report as day, month, year, or month, year. If more than one date appears on the report, use date of publication.

7a. TOTAL NUMBER OF PAGES: The total page count should follow normal pagination procedures, i.e., enter the number of pages containing information.

7b. NUMBER OF REFERENCES: Enter the total number of references cited in the report.

8a. CONTRACT OR GRANT NUMBER: If appropriate, enter the applicable number of the contract or grant under which the report was written.

8b, 8c, & 8d. PROJECT NUMBER: Enter the appropriate military department identification, such as project number, subproject number, system numbers, task number, etc.

9a. ORIGINATOR'S REPORT NUMBER(S): Enter the official report number by which the document will be identified and controlled by the originating activity. This number must be unique to this report.

9b. OTHER REPORT NUMBER(S): If the report has been assigned any other report numbers *(either by the originator or by the sponsor)*, also enter this number(s).

10. AVAILABILITY/LIMITATION NOTICES: Enter any limitations on further dissemination of the report, other than those imposed by security classification, using standard statements such as:

(1) "Qualified requesters may obtain copies of this report from DDC."

(2) "Foreign announcement and dissemination of this report by DDC is not authorized."

(3) "U. S. Government agencies may obtain copies of this report directly from DDC. Other qualified DDC users shall request through _____."

(4) "U. S. military agencies may obtain copies of this report directly from DDC. Other qualified users shall request through _____."

(5) "All distribution of this report is controlled. Qualified DDC users shall request through _____."

If the report has been furnished to the Office of Technical Services, Department of Commerce, for sale to the public, indicate this fact and enter the price, if known.

11. SUPPLEMENTARY NOTES: Use for additional explanatory notes.

12. SPONSORING MILITARY ACTIVITY: Enter the name of the departmental project office or laboratory sponsoring *(paying for)* the research and development. Include address.

13 ABSTRACT: Enter an abstract giving a brief and factual summary of the document indicative of the report, even though it may also appear elsewhere in the body of the technical report. If additional space is required, a continuation sheet shall be attached.

It is highly desirable that the abstract of classified reports be unclassified. Each paragraph of the abstract shall end with an indication of the military security classification of the information in the paragraph, represented as (TS), (S), (C), or (U).

There is no limitation on the length of the abstract. However, the suggested length is from 150 to 225 words.

14 KEY WORDS: Key words are technically meaningful terms or short phrases that characterize a report and may be used as index entries for cataloging the report. Key words must be selected so that no security classification is required. Identifiers, such as equipment model designation, trade name, military project code name, geographic location, may be used as key words but will be followed by an indication of technical context. The assignment of links, rules, and weights is optional.